RSC Publishing Faraday Discussions

FDATMOS16 Oxidative potential of size-fractionated atmospheric aerosol in urban and rural sites across Europe

Journal:	*Faraday Discussions*
Manuscript ID	FD-ART-11-2015-000196.R1
Article Type:	Paper
Date Submitted by the Author:	23-Dec-2015

Complete List of Authors:	Shafer, Martin; University of Wisconsin-Madison, Environmental Chemistry + Technology Hemming, Jocelyn; Wisconsin State Laboratory of Hygiene, Environmental Toxicology Antkiewicz, Dagmara; Wisconsin State Laboratory of Hygiene, Environmental Toxicology Schauer, James; University of Madison-Wisconsin,, Department of Civil and Environmental Enigineering

SCHOLARONE™
Manuscripts

Oxidative potential of size-fractionated atmospheric aerosol in urban and rural sites across Europe

Martin M. Shafer,[a,b,†] Jocelyn D. Hemming,[b] Dagmara S. Antkiewicz[b] and James J. Schauer[a]

[a]*Environmental Chemistry and Technology Program, University of Wisconsin-Madison, 660 N. Park St., Madison, WI 53706, USA*
[b]*Wisconsin State Laboratory of Hygiene, 2601 Agricultural Drive, Madison, WI 53718, USA.*
† Corresponding Author

Electronic Supplementary Information (ESI) available
DOI: 10.1039/x0xx00000x

In this study we applied several assays, an in-vitro rat alveolar macrophage model, a chemical ROS probe (DTT, dithiothreitol), and cytokine induction (TNFα) to examine relationships between PM-induced generation of reactive oxygen species (ROS) and PM composition, using a unique set of size-resolved PM samples obtained from urban and rural environments across Europe. From April-July 2012, we collected PM from roadside canyon, roadside motorway, and background urban sites in each of six European cities and from three rural sites spanning the continent. A Hi-Vol sampler was used to collect PM in three size classes ($PM_{>7}$, PM_{7-3}, PM_3) and PM was characterized for total elements, and oxidative activity quantified in unfiltered and filtered PM extracts. We measured a remarkable uniformity in air concentrations of ROS and especially DTT activity across the continent. Only a 4-fold difference was documented for DTT across the urban sites and a similar variance was documented for ROS, implying that chemical drivers of oxidative activity are relatively similar between sites. The ROS and DTT specific activity was greater at urban background sites (and also rural sites) than at urban canyon locations. PM_3 dominated the size distribution of both ROS activity (86% of total) and DTT activity (76% of total), reflecting both the large contribution of PM_3 to total PM mass levels and importantly the higher specific oxidative activity of the PM_3 in comparison with the larger particles. The soluble fraction of total activity was very high for DTT (94%) as well as for ROS (64%) in the PM_3. However in the larger PM size fractions the contributions of the insoluble components became increasingly significant. The dominance of the insoluble PM drivers of activity was particularly evident in the TNFα data, where the insoluble contribution to cytokine production could be 100-fold greater than that from soluble components. ROS and DTT activity were strongly correlated in the PM_3 (r=0.93), however oxidative activity was not correlated with any measured inorganic element in this size cut. In contrast, significant correlations of both ROS and DTT oxidative activity with specific groups of chemical elements were documented in the larger PM size fractions.

INTRODUCTION

Adverse health effects of ambient air particulate matter (PM) include respiratory and cardiovascular diseases, as well as cancer, contributing to an estimated 3.2 million premature deaths annually worldwide.[1–3] The effect of near roadway air pollution on human health is especially significant in major cities, with respiratory and cardiovascular diseases being implicated in response to prolonged exposure to PM.[4–8] Current regulations aiming to limit roadway-related air pollution have focused on reducing tailpipe emissions, yet recent reports suggest that all major components of PM, including metals and trace elements can potentially contribute to toxicity.[9–11] However, tailpipe emissions from mobile sources are not the major contributor to those metals as their roadway emissions are largely associated with brake wear, tire wear, and re-suspension of road dust.[12] Important metals from brake wear include Fe, Cu, Mn, Sr and Ba, while the re-suspended road dust is an important source of Pb, V and Cr, as well as crustal elements.[13–15]

Oxidative stress due to excess reactive oxygen species (ROS) production is hypothesized to be one of the unifying mechanisms underlying the adverse health effects associated with exposure to ambient PM.[16] PM has been shown to generate ROS including H_2O_2, hydroxyl and superoxide radicals and to activate redox-sensitive signaling pathways including the mitogen-activated protein kinases (MAPKs), the nuclear factor kappa B (NFκB) cascade, and the antioxidant responsive element (ARE) systems.[17–19] The downstream effects of these redox-sensitive pathways include inflammatory responses such as cytokine production.[20]

Alveolar macrophages are a part of the innate immune system function and a first line of defense against particles and pathogens entering the lungs. They are equipped with a robust NADPH oxidase system (NOX2) that generates ROS as means of defense against invading pathogens (process of "respiratory burst").[21,22] Macrophages have been shown to produce ROS in response to the PM exposure in a dose-dependent fashion.[23,24] These cells are also particularly well suited to study etiology of respiratory disease due to their instrumental role in mediating inflammatory response in the lungs. Multiple studies have demonstrated various macrophage cell lines to respond to PM exposure with a release of pro-inflammatory signals.[25–29] Recent studies reported that PM-derived water-soluble transition metals (e.g. Fe, Ni, Cu, Cr, Mn, Zn and V) significantly correlate with the oxidative potential of airborne PM across different urban areas and size ranges.[24,30] In contrast, little is known about the components of PM that are the main drivers of the inflammatory signaling induction. In this study we apply several assays, an in-vitro rat alveolar macrophage model, a chemical ROS probe (DTT), and inflammatory cytokine measure (TNFα) to examine relationships between PM-induced generation of reactive oxygen species (ROS) and PM composition, using a unique set of size-resolved PM samples obtained from urban and rural environments across Europe. We emphasize in this study geographic, site type, and particle-size contrasts in aerosol oxidative properties.

EXPERIMENTAL

Sample Collection.

PM samples were obtained from several sites in each of six geographically and climatically diverse major European Cities (Amsterdam, Frankfurt, London, Milan, Stockholm and Thessaloniki) between April and July of 2012. Within each city samples were collected from sites representing roadside canyons, roadside motorways and background urban locations. We also placed samplers at several rural locations in Northern, Central and Southern Europe to characterize the regional background aerosol oxidative activity. The Northern site was located near the North Sea and thus had a marine influence as well as capturing background from Scandinavia; the Central site was located in rural central Germany and was positioned to capture continental background; and the Southern site was located on the Southern slope of the Alps in Northern Italy and primarily reflected aerosols from the Mediterranean region. Samples were collected using Tisch (TE-230) Hi-Vol Environmental Impactor Samplers

configured for three size-cuts, and fitted with pre-cleaned mixed-cellulose ester (MCE) substrates. Samplers were operated continuously for 3-4 days at nominal flow rates of 1.2 m^3 min^{-1}, sampling 5000 m^3 of air, and collecting from 50-300 mg of PM onto the MCE filter media. Three particle size cuts were collected: a super coarse fraction including all total suspended particulate matter (TSP) with aerodynamic diameters greater than 7 microns ($PM_{<7}$), a coarse fraction containing particles with aerodynamic diameters between 3 and 7 microns (PM_{7-3}), and a fine fraction with particles less than 3 microns (PM_3).

Sample Chemical Characterization.

The samples, along with an extensive set of field blanks, were analysed with a broad range of characterization tools including magnetic-sector ICPMS (SF-ICPMS) for 50 elements; Ion Chromatography (Dionex LC20 IC) for soluble ions (K^+, Na^+, NH_4^+, SO_4^{2-}, NO_3^-, Cl^-); and several toxicity assays. Gravimetric mass was determined using microbalances operated in a temperature and humidity regulated weighing room. Static was controlled by both electronic ionizers and polonium ionization sources. Filters were sectioned in a trace element clean laboratory under HEPA hoods using ceramic tools. Each section was weighed and dedicated to a specific analysis protocol. Total elements were determined by magnetic sector ICPMS (Thermo-Finnegan Element 2) after complete solubilization of the filter-collected PM using a microwave-aided mixed acid digestion. Quantitative recovery of over 50 elements was verified through inclusion of several Certified Reference Materials in each analytical batch. Details of these methods are given in Okuda et al., 2014[31]; Shafer et al., 2012[32] and Hu et al., 2009[33].

PM Extract Preparation.

Sections of the MCE filter samples were extracted with high-purity Milli-Q (18 mΩ) water using an initial sonication period of 15 min followed by 16 h of continuous agitation at room temperature in the dark and another 15 min sonication, followed by 1 min of agitation by a vortex mixer. An aliquot of sample suspension (referred to here as “Unfiltered” samples) was subsequently portioned and distributed for various assays/analyses and then processed through 0.22 µm polypropylene (referred to here as “Filtered” samples) syringe filters. Filtration at 0.22µm provides an operationally defined water soluble fraction, however the potential inclusion of colloidal material in the filtrate precludes defining this fraction as containing truly dissolved species. All samples were buffered with Salts Glucose Media (SGM) prior to use in the in-vitro assays.

DTT.

The DTT assay was used to measure the oxidative potential of particles and has frequently been applied to atmospheric PM and major PM sources. It is a purely chemical method, no cells are involved, and in the assay redox-active chemicals in the PM oxidize added DTT to its disulfide form and the linear rate of DTT loss is equated to the oxidative activity of the PM. In the

process an electron transfer from these redox active species to molecular oxygen occurs, forming superoxide which can react to form other ROS species (e.g. hydrogen peroxide and hydroxyl radical)[34]. This ROS cascade is similar in many respects to the oxidative burst initiated by superoxide formation in the mitochondria of cells. The technique is responsive to redox-active organic compounds (e.g. quinones) and to many metals; however the metals are significantly less efficient at oxidizing DTT compared to reactive quinones. The method used for this study was based on Cho et al. 2005.[35] Up to four dilutions of PM suspensions from water extracts were added to 1.2 mL cluster tubes with volume totaling 445 µL. Samples were allowed to equilibrate in a 37^{o}C water bath prior to initiating the reaction. The reaction was initiated by adding 55 µL of a mixture of 1 M KPO4 buffer (pH 7.4) plus 10 mM DTT mixture, for a final concentration of 0.1 M and 0.1 mM, respectively. This incubation mixture (IM) was immediately vortexed and 25-µl per well of IM (in triplicate) was removed and added to a 96-well plate containing 25 µl 10% trichloroacetic acid to quench the reaction for the time= 0 time point. The cluster tubes containing the IM were returned to the water bath with subsequent 25 µL aliquots removed as described above at 15, 30, 45 and 60 minutes. After samples for all time points were collected, 100 µL Tris-HCl (0.4M, pH 8.9) containing 20 mM of EDTA and 0.24 mM DTNB was added to each well. The plate was mixed for 20 seconds prior to absorbance reading at 412 nm (optical density of 2-nitro-5-thiobenzoic acid) and 650 nm (reference wavelength) on an M5e plate reader (Molecular Devices, Sunnydale, CA). The rate of DTT consumed was determined by converting OD readings to nmoles DTT remaining. The slope of DTT consumed of type I water alone (untreated control) was subtracted from the slope of the PM containing samples and corrected for the dilution used.

ROS Production Determination.

The ROS activity of the PM extracts was measured using a previously described method employing an in-vitro rat alveolar macrophage (NR8383) model and a wide spectrum ROS probe.[23] Cellular ROS encompass many chemical species, including the oxygen and hydroxyl radicals as well as other reactive forms of oxygen such as hydrogen peroxide and singlet O_2. Oxidative stress in cells results when ROS concentrations exceed the capacity of innate antioxidant systems. The NR8383 cell line manifests all of the typical characteristics of a normal primary macrophage cell and is highly responsive to particulate and microbial stimuli by phagocytosis and to soluble species. Importantly, these macrophages display oxidative burst and secrete a wide range of pro-inflammatory cytokines. In recent epidemiology studies, the assay has been shown to have a robust association with both airway and systemic inflammation biomarkers that lead to adverse health effects.[36,37] In summary, the membrane-permeable 2′,7′-dichlorodihydrofluorescein diacetate (DCFH-DA) probe enters the macrophage cell and is de-acetylated by cytoplasmic esterases, which then allows ROS species to convert DCFH to its fluorescent form, DCF. The DCFH probe is sensitive to the broad spectrum of ROS species produced intra-cellularly. This enables the quantification of biologically mediated production of ROS in response to cellular stimulation (e.g. PM exposure). The rat alveolar macrophage NR8383 (CRL-2192™) cell line was obtained from ATCC (Manasses, VA, USA) and cultured

according to the manufacturer's instructions: in Hams F12 medium (Sigma Aldrich, St. Louis, MO) supplemented with 15% fetal bovine serum (FBS; Hyclone, Fisher, USA) and sodium bicarbonate (1.176 g L-1). Cells were maintained at 37°C in a humidified incubator supplied with 5% CO_2. Non-adherent macrophage cells were harvested, centrifuged and resuspended in SGM to obtain a concentration of 1,000 cells/µL. Subsequently 100 µL of this suspension was seeded into 96-well plates and cells were allowed to adhere for 2 h at the standard conditions of 37ºC and 6% CO_2. Following the cell adhesion period the buffer medium was aspirated and the SGM-buffered unfiltered and filtered PM extracts (mixed with a small volume of DCFH-DA solution (45 µM final concentration) were added to the cells. This exposure was carried out for 2.5 h under standard culturing conditions, after which the fluorescence intensity of each well was determined at 488 nm excitation and 530 nm emission using an M5e microplate reader (Molecular Devices, CA, USA). Raw fluorescence data was blank-corrected and normalized to the Zymosan (ZYM) positive controls (β-1,3 polysaccharide of D-glucose from Sigma Aldrich, MO, USA) to enable cross-study comparisons. Multiple dilutions of each sample were run, each in triplicate, to establish a linear portion of the dose response.

TNFα Production Determination.

TNFα is a cytokine (cell signaling protein) involved in systemic inflammation, where its' primary role is regulation of immune cells. It is produced primarily by activated macrophages (like NR8383), though other cell types (e.g. neutrophils and endothelial cells) can also produce TNFα. The cytokine binds to two receptors (TNFR1 and TNFR2) found in many tissues and cells of the immune system and subsequently activates several major pathways (including NF-κB, MAPK/JNK) involved in cell survival, proliferation, inflammatory responses, and both anti- and pro-apoptotic factors. TNFα secreted by the NR8383 macrophages after 6 hours of exposure to the PM extracts was measured in the supernatant of the exposure solution by enzyme-linked immunosorbent assay (ELISA). Supernatants were pipetted from the cell exposure wells, centrifuged (1,600 g for 15 minutes at 4°C) and the particle-free supernatants immediately frozen (-30°C) until the ELISA was performed. The ELISA was carried-out with BD OptEIA Rat TNFα kits following the manufactures protocols. Absorbances were read in a Molecular Devices M5e plate reader at 450 nm and using 570 nm as correction/reference wavelength. Calibration was performed with authentic standards over the concentration range of 31 to 2000 pg TNFα/mL. Every standard, sample, and control sample was run in duplicate.

Statistical Analysis.

Basic statistical analyses, including Spearman Correlation analysis were performed with the SigmaStat module integrated into SigmaPlot (version 13.0, Systat Software Inc. 2014).

RESULTS

Aerosol PM Concentrations

Aerosol PM concentrations (Fig. 1S, ESI) ranged from <10 μg m^{-3} (Stockholm urban background) to over 75 μg m^{-3} in the urban roadside canyons of London and Thessaloniki. PM concentrations at the rural sites were relatively low (mean = 15.3 μg m^{-3}) and consistent (± 1.5 μg m^{-3}). The average PM concentration across all cities and sites was 31.5 μg m^{-3} with urban background levels consistently in the 10-20 μg m^{-3} range. The large majority of the PM mass was present in the fine (PM_3) size cut (Fig. 1S, ESI), with the coarse (PM_{7-3}) and super-coarse ($PM_{>7}$) size fractions contributing about equal to the remainder of the PM.

ROS and DTT Activity – Study Site Comparison

The size-resolved ROS activity of unfiltered and filtered PM extracts, expressed in terms of air concentrations is shown in Fig. 1 and Fig. 2. The ESI presents this data in more detail (Fig. 2S and Fig. 3S, ESI). The ROS activity of unfiltered extracts across all 17 sites ranged from 25 to 106 μg ZYM /m^3, averaging 69.6 ± 23.1, with a median value of 73.0. Filtered extract activity was substantially lower (range = 11 to 89 μg ZYM /m^3, averaging 42.6 ± 26.6, with a median value of 36.2. ROS activity was generally similar in all cities studied. The variation in ROS activity across all sites of 30% (unfiltered) and 60% (filtered) is relatively small, considering this reflects a wide range of anthropogenic influence, from heavily traveled urban roadway canyons to rural locations. Variation in ROS activity within site types (urban background, urban canyon/roadside, rural) was substantial (Fig. 2), however on average urban background sites exhibited the highest ROS concentrations (median = 90 μg ZYM /m^3), followed by urban canyon sites (64 μg ZYM /m^3) and rural sites (54 μg ZYM /m^3). In all cites except Thessaloniki, the measured ROS concentrations at the canyon sites was less than that at background sites – a trend that was particularly evident in the filtered extracts. The relatively high rural and urban background site concentrations (e.g. rural ROS activity is nearly twice as great as canyon site activity in filtered PM extracts) reflect primarily the higher specific ROS activity (see following section) of PM in rural and background sites.

The size-resolved ROS activity of unfiltered and filtered PM extracts, normalized to PM mass concentrations is shown in Fig.1 and Fig. 3. The ESI presents additional detail on the mass normalized ROS activity (Fig. 4S and Fig. 5S, ESI). Normalizing the ROS activity to PM mass results in a metric that reflects the intrinsic oxidative activity of the PM (in contrast to the air volume normalization (above) that provides information on potential human exposure levels). The intrinsic activity of unfiltered extracts across all 17 sites ranged from 740 to 9200 μg ZYM /mg, averaging 3130 ± 2380, with a median value of 2175. The variation across sites in the mass normalized data (76%) is greater than the corresponding air volume data. Again, variation in ROS activity within site types was substantial (Fig. 3), however on average urban background sites exhibited the highest ROS intrinsic activity (median = 3700), followed by rural sites (2200)

and then urban canyon sites (1750). The 2-fold lower activity in the canyon sites compared with background and rural sites is remarkable. In each city sampled the intrinsic activity of the background sites was greater than at canyon sites – in several cities by nearly 5-fold. PM specific activity was lowest in canyon sites of London, Milan and Thessaloniki (those greatest density of traffic) and highest at urban background sites of Stockholm, Frankfurt and London. PM from the central Europe rural site also exhibited high specific ROS activity.

The size-resolved DTT activity of unfiltered and filtered PM extracts, expressed in terms of air concentrations is shown in Fig. 4. The ESI presents this data in more detail (Fig. 6S and Fig. 7S, ESI). The air concentrations of aerosol DTT activity of unfiltered extracts across all sites ranged from 0.14 to 0.62 nmole/min/m^3, averaging 0.287 ± 0.132, with a median value of 0.249. Filtered extract activity was only marginally lower (range = 0.11 to 0.51 nmole/min/m^3, averaging 0.254 ± 0.118, with a median value of 0.216 (just 13% lower than in unfiltered extracts). DTT activity was remarkably similar in most cities – only Milan and Thessaloniki exhibited activity significantly greater than the median. Even more so than in the ROS data, the variation across sites is exceptionally low. Variation in DTT activity within site types was evident (Fig. 6), but not as great as with ROS activity, and on average urban background sites exhibited the highest DTT concentrations (median = 0.27), followed by urban canyon sites (0.25) and rural sites (0.17). In all cites except Thessaloniki, the DTT concentrations at the canyon and background sites were nearly equivalent.

The size-resolved DTT activity of unfiltered and filtered PM extracts, normalized to PM mass concentrations is shown in Fig. 4. The ESI presents additional detail on the mass normalized DTT activity (Fig. 8S and Fig. 9S, ESI). The intrinsic activity of unfiltered extracts across all 17 sites ranged from 5.2 to 20.0 nmole/min/mg, averaging 10.6 ± 4.3, with a median value of 9.7. Unlike with the ROS data, where mass normalization increased the variation across sites, mass normalizing the DTT data actually reduced the variance (40% versus 46%) compared with the corresponding air volume data. Again, variation in DTT activity within site types was substantial (Fig. 6), however on average urban background sites exhibited the highest DTT intrinsic activity (median = 11.5), followed by rural sites (8.5) and then urban canyon sites (7.5). With the exception of Thessaloniki, in each city sampled the intrinsic activity of the background sites was equal to or greater than at canyon sites, but the contrast was not nearly as great as with ROS activity. In very similar findings to the ROS, PM specific activity was lowest in canyon sites of London, Milan and Thessaloniki and highest at urban background sites of Stockholm and London. PM from the central Europe rural site also exhibited high DTT activity. Overall, the pattern of DTT activity across study sites generally tracked that of ROS.

TNFα Production -- Site Comparison

Expressed on an air volume normalized basis the TNFα production from the unfiltered PM_3 samples from Thessaloniki urban background (578,700 ng TNFα/m^3 and London urban canyon

(525,300 ng TNFα/m^3) sites were over 5-fold greater than all other PM_3 sites (Table 1) In the filtered PM_3 samples, the highest TNFα induction was observed in the London sample (9,300 ng TNFα/m^3), followed by the Milan urban background site (7,000 ng TNFα/m^3). Within the rural site PM_3 samples, the TNFα production was lowest in the North Rural site (unfiltered = 7,400 ng TNFα/m^3, filtered = 989 ng TNFα/m^3), followed by the Central location and the highest values observed for the South Rural site (both total and filtered fraction, normalized to mass, as well as to air volume).

The highest intrinsic (i.e. PM mass-normalized) TNFα-inducing activity of unfiltered PM_3 was observed at the Thessaloniki urban background site (28,900 pg TNFα/mg PM), followed by the London urban canyon site (10,900 pg TNFα/mg PM) and then the Frankfurt urban background site (8,700 pg TNFα/mg PM). However, for the filtered PM_3 fraction the highest activity was observed at the Stockholm urban background site (591 pg TNFα/mg PM), followed by Frankfurt urban background (447 pg TNFα/mg PM) and Amsterdam urban background sites (Table 1). Interestingly, for the PM_{3-7} size fraction, the Thessaloniki PM_{3-7} site was the most active on both an air volume (33,200 ng TNFα/m^3) and PM mass normalized basis (9610 pg TNFα/mg PM).

Particle Size-Resolved Analysis

As clearly shown in Fig. 7, the PM_3 dominates the air concentrations of ROS. Across all 17 sites, in unfiltered PM extracts, the PM_3 represents 86% of total activity, with the PM_{7-3} contributing on average 9% and $PM_{>7}$ just under 5%. The corresponding percentages are 91%, 7% and 2% for the filtered extracts. The dominance of the PM_3 is evident in all site classes (FIGURE XX) and the fraction of PM_3 is remarkable consistent; 87%, 84%, and 87% for urban background, urban canyon and rural sites respectively. The contribution of the super coarse ($PM_{>7}$) was greater than average at the Milan urban background (10%) and Thessaloniki sites (10% background and 14% canyon).

Similar to the ROS findings, air concentrations of DTT (Fig. 8) are also dominated by the PM_3. Across all 17 sites, in unfiltered PM extracts, the PM_3 represents 76% of total activity, with the PM_{7-3} contributing on average 17% and $PM_{>7}$, 7%. The corresponding percentages are 84%, 11% and 5% for the filtered extracts. The dominance of the PM_3 is particularly evident at the urban background and rural sites (Fig. 8, Fig. 3) with contribution percentages of 81 and 83% respectively. A significantly lower PM_3 contribution was observed in the canyon sites (67%) with a corresponding large increase in the contribution of PM_{7-3} (23%), indicating a major coarse input from vehicle-sourced emissions (tire/brake wear and resuspended road dust). This coarse contribution was most evident at the canyon sites in London and Thessaloniki (the most vehicle influenced sites).

There is a clear trend of increasing ROS specific activity with smaller particle size (Fig. 9). Across all 17 sites, in unfiltered PM extracts, the median specific activity of the PM_3 was 2600 μg Zymosan (ZYM)/mg, 1800 in the PM_{7-3} and just 750 in the $PM_{>7}$ (4-fold lower than in PM_3).

Several high "outlier" values drive the arithmetic average higher than the median and these corresponding activities were 4000, 2000 and 1050 μg ZYM/mg. The particle-size dependence of ROS specific activity is evident in all three major site classifications (Fig. 3). The trend is seen most dramatically in the urban background sites (5600, 1800, 850 μg ZYM/mg in the PM_3, PM_{7-3}, and $PM_{>7}$ respectively; but also strongly evident in the rural sites (3400, 1950, 550) and canyon sites (1850, 1400, 750). The highest PM_3 specific activities were measured at urban background sites in Stockholm (12400), Frankfurt (8300), London (6600) and Amsterdam (5600) (Fig. 4S). ROS specific activity at most of the other urban sites was typically in the 1000-2000 μg ZYM/mg range. Rural sites exhibited ROS specific activities in the 1000-3000 range, though the PM_3 at the central Europe rural location had the 2nd highest measured activity (9050).

The trend of DTT specific activity with particle size (Fig. 10) is a bit more complex than that observed with ROS, resulting primarily from an input of DTT active materials into the PM_{7-3} size class in the urban canyon sites. Across all 17 sites, in unfiltered PM extracts, the median specific activity of the PM_3 was 9.5 nmoles/min/mg, 13.5 in the PM_{7-3} and just under 5 in the $PM_{>7}$ (2-fold lower than in PM_3). As with the ROS data, several high "outlier" values drive the DTT arithmetic average higher than the median and these corresponding activities were 12, 13.5 and 7 nmoles/min/mg. When these data are parsed into site types, the influence and unique trends in the urban canyon sites becomes very clear (Fig. 6). While the trends in specific activity as a function of particle size at the urban background (15.5, 12.5, 4) and rural (14, 7.5, 5) (PM_3, PM_{7-3}, $PM_{>7}$ respectively) sites are very similar to that observed with the ROS data (consistent decrease with increasing particle size), the trend is dramatically different at the canyon sites with median PM_{7-3} activity of 20.5 compared with 7.5 in the PM_3 and 7 in the $PM_{>7}$. The canyon sites/cities contributing most significantly to this "elevated" PM_{7-3} specific activity were Stockholm (25-30), Frankfurt (22) and Thessaloniki (20.5). The highest PM_3 specific activities were measured at urban background sites in Frankfurt (27), Stockholm (18) and London (17) (Fig. 8S). DTT specific activity at most of the other urban sites was typically in the 5-15 nmoles/min/mg range. DTT activity at the rural sites was also typically in this 5-15 nmole/min/mg range, however just like with ROS the central Europe rural location exhibited a relatively high activity (22 nmoles/min/mg).

TNFα. Overall, TNFα secretion was substantially higher in PM_3 than in PM_{3-7}, whether normalized to air volume or PM mass. The greatest size contrast was in the air volume normalized total fraction data, followed by air-volume normalized filtered fraction data and mass-normalized total PM (Table 1). Of note, the Milan UBI mass-normalized sample exhibited the opposite trend, with PM_{3-7} eliciting higher production of TNFα than PM_3 in both total and filtered fractions. However, this trend was not observed for the corresponding air-volume normalized data.

Unfiltered-Filtered Analysis

ROS. Averaged over all sites and particle size classes, the fraction of aerosol ROS activity that is water soluble was 60% (the median value, 57.5%, is similar, indicating a normal type distribution) Fig. 11. At several of the urban background sites, the soluble ROS percentage approached 100% (Amsterdam = 96%, London = 94%). Importantly, the soluble percentage was also consistently very high at the rural sites. Urban canyon sites exhibited the lowest water solubility, with London, Milan and Stockholm all in the range of 20-30%. When broken out by particle size class (across all 17 sites), there is a clear trend of decreasing median water solubility with increasing particle size (59.5% in PM_3, 30% in PM_{7-3}, and 25% in $PM_{>7}$) (Fig. 11). Many of the $PM_{>7}$ samples exhibited exceptionally low water soluble ROS fractions of 10% or lower (Frankfurt and Stockholm urban background sites and London, Milan, Stockholm and Thessaloniki urban canyon sites). In contrast, the $PM_{>7}$ soluble percentage at the rural sites was very high (>90% in two locations).

DTT. Overall, water soluble metrics of the DTT data exhibited similar trends to the ROS data, though the absolute water soluble percentages were significantly higher. Averaged over all sites and particle size classes, the fraction of PM DTT activity that is water soluble was 83% (median = 84%) Fig. 12. At seven of the 14 sites, the soluble DTT percentage was greater than 90%. Water solubility was slightly higher in the urban background locations. As seen with the ROS data, the soluble percentage was also consistently very high at the rural sites. Urban canyon sites exhibited substantially lower water solubility, with London (55%) and Thessaloniki (65%), the lowest. When broken out by particle size class (across all 17 sites), there is, like with the ROS data, a clear trend of decreasing median water solubility with increasing particle size (93.5% in PM_3, 56% in PM_{7-3}, and 50% in $PM_{>7}$) (Fig. 12). With the exception of sites in London and canyon site in Thessaloniki, all PM_3 water soluble fractions were >90%. The lowest soluble DTT percentages were measured in the $PM_{>7}$ from urban canyon sites (London 38%, Milan 32%, Stockholm 27%, Thessaloniki 20%) (Fig. 11S, ESI). In contrast, the $PM_{>7}$ soluble percentage at the rural sites was high (70-80% across all locations).

TNFα. Production of TNFα was especially sensitive to the presence of particles, with ratios of total to filtered values as high as 120 (Table 1). The filtered fraction was typically at least 10-fold lower in activity than the unfiltered samples in both the PM_3 and PM_{3-7} size classes. The one exception was at the Central Rural site where the unfiltered and filtered activities of the PM_{7-3} were similar.

Association of Oxidative Activity with Elemental Composition of PM

In Table 2 we present a summary of the Spearman Correlation Coefficients between ROS and DTT activity and the elemental composition of the PM. From the 50 element SF-ICPMS analysis of TOTAL elemental composition of the PM in the three particle size cuts (refer to Fig. 12S, ESI), we selected the 28 elements with concentrations above 10 μg/g and generated the Spearman

Correlation Coefficients on the size-resolved ROS and DTT data. Chemical elements are ranked in Table 2 by the median elemental concentration in the bulk (i.e. reconstructed) PM. The major PM bulk components, alkaline earths (Ca, Mg), alkali metals (Na, K), S (sulfate), and Al (aluminosilicate) are present at concentrations in the range of 1-7%. Iron (Fe) is by far the most abundant transition metal, with concentrations ranging from 2% in the PM_3 to over 5% in the coarser size fractions. Titanium (Ti), another aluminosilicate tracer is present at concentrations of 0.1-0.2%. The second most abundant 1st row transition metal is Cu, followed by Zn, and then Mn, with concentrations ranging from 800 to 2000 μg/g. Barium (Ba), a good tracer of brake wear is present at levels comparable to that of Zn and Mn. The 1st row transition elements, Cr, Ni, and V are found at levels of 300, 100, 60 μg/g respectively. Iron, Cu, Mn, Ni, and V are redox active in environmental PM. The semi-metals Sn and Sb, along with Pb fill out the elements present at levels >100 μg/g (200, 150, 200 μg/g respectively). With the exception of V and Zn ("soft" elements with greater mobility and water solubility), all the minor/trace elements mentioned above are strongly enriched in the coarser PM size fractions.

ROS and DTT activities were strongly (>0.9) associated in the PM_3, exhibiting a Spearman coefficient of r= 0.93. Association between ROS and DTT was also evident in the largest size cut ($PM_{>7}$, r=0.69), but no correlation was found in the PM_{7-3} size cut.

No chemical elements were associated with ROS and DTT activity at a level of correlation above r=0.7 in the PM_3 size cut. In fact, S was the only element that exhibited a marginal correlation (>0.5) with ROS and DTT in the PM_3. In contrast, several elements exhibited good (>0.7) to marginal (>0.5) correlation with ROS and DTT in the larger PM size fractions. Potassium (K) (r=0.95), a biomass burning tracer, and Rb (r=0.71) were associated with ROS activity in the PM_{7-3} size cut. Magnesium (r=0.61), Li (r=0.61), Al (r=0.56) and Ti (r=0.52), all dust/aluminosilicate tracers exhibited marginal correlations with ROS. Interestingly, both K and Rb were NOT correlated with ROS in the super-coarse ($PM_{>7}$) fraction. Elements associated with ROS activity in the largest size cut ($PM_{>7}$) included most of the aforementioned crustal elements (Mg, Al, Ti) along with Ca (r=0.67), but maybe more importantly a large suite of redox active transition metals exhibited good to marginal correlations (Mn: r=0.73, Ni: r=0.73, V: r=0.66) with ROS. Arsenic (As) (r=0.71) and Co (r=0.64) also were associated with super-coarse ROS activity. A completely different suite of elements from that correlated with ROS was associated with DTT activity in the PM_{7-3} size cut. Iron (r=0.79), Sn (r=0.79), Cu (r=0.76), Sb (r=0.73), and Ba (r=0.70) all non-tailpipe vehicle emission tracers, exhibited good correlations with DTT. Also showing marginal correlations to DTT in the PM_{7-3} were Mo (r=0.68), Mn (r=0.66), Zn (0.62), Ce (r=0.60), As (r=0.59), Cr (r=0.55) and La (r=0.50). Only one element, As (r=0.71) exhibited a good correlation with DTT in the $PM_{>7}$ fraction, however a very large number of elements exhibited marginal correlation with DTT in this particle size cut. This included all of the trace elements correlated in the PM_{7-3} fraction, with the addition of several crustal tracers (Al, Ti, Sr, and Li).

DISCUSSION

Air Concentrations of Aerosol ROS, DTT and TNFα Activity

We measured a remarkable uniformity in air concentrations of ROS and especially DTT across the continent. Only a 4-fold difference was documented for DTT across the urban sites (0.14 to 0.62 nmole/min/m^3) and a similar variance was documented for ROS (25 to 106 μg ZYM/m^3). Rural site DTT activity clustered in a very narrow range, just 2-fold lower than at the urban sites. ROS activity at the rural sites exhibited a greater range, spanning a good portion of the range measured at the urban sites. This overall similarity reflects a relatively small variation in PM concentrations across the study sites and implies that chemical drivers of oxidative activity are not too dissimilar between sites. DTT levels of this order are also consistent globally, e.g. DTT concentrations in samples collected in Beijing by Liu et al.[5] ranged between 0.1-0.5 nmoles/min/m^3 - strikingly similar to the levels measured in the current study of European sites. The significant oxidative potential of the PM at urban background and rural sites suggests that the oxidative stress health implications of aerosol exposures may not necessarily be only an urban problem. In contrast to the ROS and DTT findings, the air concentrations of TNFα induction activity of the aerosol exhibited quite large contrasts between sites. Nearly an 80-fold range (7,000 to 580,000 ng TNFα/m^3) was measured.

PM_3 dominated the size distribution of DTT activity (76% of total) with coarse and super-coarse size fractions contributing much smaller to total activity (17% and 7% respectively). Analogous trends were observed in the ROS data (86% of total activity in the PM_3), with even smaller average contributions from the larger size PM (9% and 7% in PM_{7-3} and $PM_{>7}$ respectively). This finding reflects both the dominance of PM_3 aerosol concentrations and higher specific activity of the PM_3 aerosols. At the urban canyon sites there is a significant contribution of oxidative activity from the PM_{7-3} size fraction, likely sourced from non-tailpipe vehicle emissions. Clearly though, reduction of the risk from PM oxidative activity should focus on controlling PM_3 emissions.

Specific Activity of Aerosol ROS, DTT and TNFα

The aerosol at urban background locations exhibited greater specific activity than that present in urban canyon locations, though the contrast is maybe less than one might expect given differences in levels of potential drivers of oxidative activity. Averaged across all sites in the particle-size summed aerosol, a 2-fold contrast in ROS activity (3700 versus 1750 nmoles/min/mg) was measured, and DTT activity at urban background sites averaged 35% higher than at urban canyon sites. Significantly, rural aerosol exhibited DTT and ROS specific activities comparable to that measured in urban background aerosol. These finding may belie expectations and clearly suggests that some of the major drivers of oxidative activity are regional in nature and distribution and not, for example, dominated by fresh emissions associated with vehicles. It is likely that aging of the aerosol is an important factor in generating

oxidative potential. This hypothesis is supported by several recent publications that document that oxidation ("aging") processes in the atmosphere produce species with greater oxidative activity.[38,39] Platt et al. 2014[38] demonstrated in dedicated chamber studies that oxidation processes produced secondary organic aerosol from vehicle exhaust with dramatically greater ROS activity than primary emissions; and similarly Saffari et al. 2015[39] documented that photochemical processing and secondary organic aerosol formation were the dominant drivers underlying the ROS activity in PM transported downwind to a location distant from primary generation source.

In the fine PM fractions (i.e. $PM_{2.5}$ or PM_3) our European samples exhibited a range in PM mass normalized DTT activity from 4-27 nmoles/min/mg PM, very similar, if slightly on the low side of what has been reported worldwide. For example: samples from Mexico City were between 5-40 nmoles/min/mg PM;[40] samples from the Netherlands ranged from 40-214,[41] samples from the Los Angeles Basin ranged from 21-75 nmoles/min/mg PM,[42] and samples from various sites in the Southeastern United States averaged about 35 nmoles/min/mg PM.[43] A study conducted in Thessaloniki[44] measured DTT in PM_{10} at a heavy traffic site and results ranged from 18-60 nmol/min/mg PM. The samples we collected in Thessaloniki were lower, at 7.5 nmol/min/mg PM.

This finding of general consistency in DTT levels across large spatial and anthropogenic gradients (rural, urban, distance from industry and roadways) is significant and given the variability in extraction and assay techniques as well as samples collected worldwide under a wide range of environmental conditions, it is striking that DTT values are in the same general range. Research is needed to further characterize the chemical species in PM that the DTT assay is responsive to and whether these species are relevant drivers of adverse human health outcomes. The efficacy of an oxidative stress assay in this context depends in large part on its ability to capture the influence of a large spectrum of health relevant species, and if this consistency is linked to a small sub-set of species, then the utility of the assay may be reduced.

The contrast between sites in macrophage ROS activity was larger than that measured in the DTT assay. A greater than ten-fold difference was seen in the mass-normalized macrophage ROS for these European sites (using data from the reconstructed pooled PM sizes) compared with a four-fold difference for the DTT assay. Contrasts in ROS activity between sites are even larger within a specific PM size class. Saffari et al.[30] summarized macrophage ROS results from the literature and found large differences in mass-normalized ROS activity between sites. For example, the ROS activity from samples collected in Los Angeles and Thessaloniki were low (483 and 572 μg ZYM/mg PM), however, the ROS activity from samples collected in Milan and Beirut were 25-50 times higher. Two other measures of oxidative potential (electron spin resonance and ascorbate depletion) also show more contrast between sites than does DTT consumption.[45] While the macrophage ROS assay is a more biologically relevant model to address oxidative activity of aerosol PM, and several studies have shown direct predictive power in human health metrics,[36,46,47] further studies are needed to assess whether the greater sensitivity and

selectively of the assay make it the preferred approach for assessment of potential human health impacts.

For Urban background and rural locations there is a general increase in DTT specific activity with decreasing particle size. A 3-fold difference between PM_3 and $PM_{>7}$ was measured for DTT and an even greater difference (5-fold) was measured between these particle size classes for ROS. However, for the Urban Canyon sites PM_3 and PM_{7-3} are comparable (if not higher in PM_{7-3}, especially for DTT) for both DTT and ROS. Only in the $PM_{>7}$ is a small decrease observed. As noted above this likely reflects an input of non-tailpipe vehicle emissions into the coarse PM_{7-3} size fraction. The trends in specific activity of ROS and DTT as a function of particle size at the urban background and rural sites implicates chemical drivers that exhibit a preference for smaller aerosols, e.g. more volatile, combustion associated metals, BC, and certain organic species. Active surface area contrasts between the particle size classes may also play a role.

Our finding that DTT activity was greatest in the PM3 fraction is consistent with numerous other studies in which fine PM fraction DTT activity was shown to be the highest. For example, De Vizcaya-Ruiz et al.[40] measured DTT activity in PM from three regions of Mexico City and found that DTT in the fine ($PM_{2.5}$) was about twice that found for the coarse $PM_{2.5-10}$, similar to the ratio documented in this study. PM of three size classes (0.18µm, <2.5µm, 2.5-10 µm) collected from diverse sites in the Netherlands were evaluated for DTT activity by Steenhoff et al.[41] The mass normalized DTT activity from the <2.5 µm size class was up to 3.7 times higher than the coarse size except for the stop and go traffic site where they were equal (a similar phenomenon was observed in our urban canyon sites (see above). At two sites (stop and go traffic and an underground tunnel) the highest mass-normalized DTT activities were in the ultrafine <0.18 µm fraction. Studies in California by Cho et al. and Ntziachristos et al. found the ultrafine PM (<0.15 µm) generated the highest DTT activities, followed by fine (<2.5 µm) and coarse (2.5-10 µm) across all sites tested.[35,42] Charrier et al. further narrowed the ultrafine size class and determined that DTT activities were higher in 0.17-1 µm fraction than they were in the <0.17 size class for the samples they collected in the central valley of California.[48]

Similarly, our finding that cellular ROS activity was highest in the PM_3 fraction is corroborated in by other studies. In New York, coarse ($PM_{2.5-10}$) and fine ($PM_{<2.5}$) were collected from three rural and two urban sites.[49] ROS was significantly higher for the cells exposed to $PM_{<2.5}$ at the urban sites, but there was no significant difference between the coarse and fine fraction for the rural sites. Super coarse ($PM_{>10}$) samples were collected at one rural and one urban site. ROS response to the super coarse sample was lowest, although only significantly so for the urban site. In samples from Los Angeles, Wang et al.[50] collected course, $PM_{2.5}$, and ultrafine PM samples from an urban site. Alveolar macrophages (NR8383) exposed to $PM_{2.5}$ extracts exhibited higher ROS activity than macrophages exposed to either coarse or ultrafine PM on a per air volume basis.

Soluble versus Insoluble Activity of Aerosol Extracts

The soluble (filterable) activity was comparable to total (unfiltered) activity for DTT (94%) in the PM_3. The soluble ROS activity fraction was also relatively high (64%) in the PM_3, but a much greater range among sites in the soluble fraction was observed. These findings suggest that the drivers of activity in this size cut are readily soluble and that the insoluble component is either small and/or inactive. However in the larger size fractions the contributions of the insoluble components become increasingly more significant as PM size increases - this trend is particularly evident in the ROS data. The overall effect on oxidative activity may simply reflect a change in particle chemistry (to more insoluble components that are also active) but may also reflect a different mode of oxidative activity generation. Overall, in each of the size fractions, the ROS soluble activity fraction was 20-30% lower than with the DTT.

ROS – DTT Interrelationships

As detailed in the results presentation, there are overall generally similar trends in the ROS and DTT data in regards to particle size distribution, with both exhibiting fairly strong inverse trends of oxidative activity with PM size. Trends in the water solubility of oxidative activity are also similar, though the absolute magnitude of the DTT activity solubility is substantially greater than with ROS activity. When parsed into site types, again many of the relationships are similar between ROS and DTT.

To provide a more quantitative picture of ROS – DTT relationships, the site pooled, particle-size resolved data (expressed both in terms of activity per air volume and activity per mg of PM) were regressed. There is a good correlation between intrinsic activity of ROS and DTT in the PM_3, both for unfiltered (r^2 = 0.75) and filtered extracts (Fig. 13S, ESI). There is a significant intercept on the DTT axis, indicating that some chemical oxidative activity is present without any ROS activity. Correlations of intrinsic ROS and DTT in the coarser size fractions are poorer than in the PM_3, particularly in the PM_{7-3} (where DTT is especially active in the canyon sites), but $PM_{>7}$ correlations are fair, especially considering the low activity of much of the data Fig. 14S, ESI). Relationships between the air volume-normalized (i.e. per m^3) PM_3 ROS and DTT data are limited at best, with the unfiltered data exhibiting an r^2 of 0.46. The filtered data show little to no correlation. There are hints of underlying relationships in the coarser size fractions, however a few “outliers”, particularly in the PM7-3 fraction, seriously degrade the correlations.

Drivers of ROS and DTT Activity

In contrast to several studies,[30,51] which document associations between PM oxidative activity and inorganic elements (particularly those associated with traffic emissions and fuel/oil combustion) in fine PM, we observed only poor correlations between any of the 28 elements and ROS and DTT activity in the PM_3 size cut. Only S exhibited a marginal (r=0.58) correlation

(with both ROS and DTT) in this size fraction. ROS and DTT are strongly correlated (r=0.93) however and it's probable that organic species are contributing to the observed oxidative activity. In contrast, we did document significant correlations between our oxidative activity metrics and several groups of elements in the larger PM size classes. In the PM_{7-3} size cut, K (r=0.95), a biomass burning tracer, and several elements associated with dust/aluminosilicates (Mg (r=0.61), Li (r=0.61), Al (r=0.56) and Ti (r=0.52) exhibited correlations with ROS. In the largest size cut ($PM_{>7}$) ROS activity was associated with a group of crustal elements (Al, Ca, Mg, Ti) and several redox active transition metals (Mn: r=0.73, Ni: r=0.73, V: r=0.66). Anthropogenic V and Ni are typically sourced from fuel oil combustion. The profile of elements associated with DTT activity was entirely different from that associated with ROS activity. In the PM_{7-3} size cut, the dominant correlations with DTT were with a group of elements sourced from non-tailpipe vehicle emissions (Fe (r=0.79), Sn (r=0.79), Cu (r=0.76), Sb (r=0.73), and Ba (r=0.70). Arsenic (r=0.71) along with all of the trace elements correlated in the PM_{7-3} fraction, and several crustal tracers (Al, Ti, Sr, and Li) were correlated with DTT in the $PM_{>7}$ size cut. Thus it would appear that in the larger particle size fractions ROS activity is likely associated with more soluble elements associated with biomass burning and fuel oil combustion and in the super coarse size fraction with crustal elements. In contrast DTT activity in the larger size PM is likely associated with less soluble vehicle/roadway sourced elements along with crustal elements.

Our TNFα data revealed that induction of this cytokine in our *in-vitro* alveolar macrophage model was almost exclusively driven by the insoluble components of the PM extracts,which is in stark contrast to the macrophage ROS production data, where we show that a large majority of the ROS activity was driven by soluble species. The ratio of unfiltered to filtered extract induction (Table 1) exceeded 100 at several sites – dramatically higher than the maximum ratio of 2 observed in the ROS data. In a recent rat study by Snow et al. animals were treated with chemically-characterized PM and showed significant increases in neutrophilic inflammation and TNFα expression due to the insoluble and total, but not soluble fraction.[26] Our data set revealed no significant correlations of TNFα levels with any of the elements measured, in agreement with reports in the literature.[52,53] Several hypotheses have been suggested to explain this TNFα production in the absence of correlation with the PM elemental composition, especially the high magnitude of expression in the unfiltered fraction of PM. One of the hypotheses suggests that the difference is due to the biogenic (particles like pollen) content of PM.[54] While some other macrophage studies show correlation between cytokine production and an endotoxin level,[52] other fail to establish that relationship and suggest other components of PM as the drivers, potentially associated with the surface of the core PM particles.[53] More research of coarse and fine PM toxicity, especially in relation to the PM's detailed chemical composition is needed to confirm any of these hypotheses.

Toxicological studies using human and animal exposure methods provide a more direct and potentially more robust approach to address aerosol driven health impacts, however the limitations of human/animal studies are many and it is clear that in-vitro assays will play an increasing role in overall toxicity assessment and as tools in advancing our understanding of

mechanisms of aerosol driven toxicity. Screening assays should be relatively rapid and inexpensive to implement and able to be standardized and implemented in laboratories in many countries. They should address the known major underlying pathophysiological mechanisms of PM-driven disease. The three assays applied in this study largely satisfy these criteria, though there are obviously substantive differences in approach and potential biological relevance as noted previously. These tools are focused primarily on measurement of oxidative stress potential (ROS and DTT) and inflammation (TNFα) (which is intimately tied to ROS) – clearly of relevance to aerosol driven human health concerns, and in that context are complementary. However they are not comprehensive in that other important pathways of aerosol toxicity (e.g. AhR activation and genotoxicty) are not addressed - that will require a larger suite of assays. A major thrust of ongoing research in the aerosol toxicity research community remains to advance our understanding of the specific chemical drivers, and complex interactions between those drivers, of pathway-specific aerosol toxicity. It is likely that pathway analysis using more specific biomarkers (e.g. expression of certain targeted genes) or reporter engineered cells will provide insight into these mechanisms. These “endpoints”, along with ROS generation, will need to be coupled with physical and chemical manipulation/treatments of PM extracts designed to isolate the influence of specific classes of chemicals/elements, if not specific agents. A greater emphasis on characterization of redox pathways, e.g. through oxidation state specific elemental characterization or with electrochemical or fluorogenic probes, should aid in the identification of active chemical species. However application of the macrophage ROS and DTT assays to a much broader array of aerosol types from urban and rural areas across the globe – an application these assays are ideally adapted for, would also provide critical new information. Coupled with detailed chemical analysis this approach would not only reveal the overall oxidative potential of a wider range of aerosols, but also help direct more targeted laboratory studies into the role of specific chemical agents.

ACKNOWLEDGEMENTS

The authors offer many thanks to the chemists from the WSLH Trace Element Research group, especially Pam Skaar and Joel Overdier. We wish to also express our gratitude to many supportive colleagues and friends from the Environmental Toxicology and Flow Cytometry groups at the WSLH. We also appreciate the field sampling efforts of students and staff from the UW-Madison ET&C program and colleagues at each sampling location. We thank the International Platinum Association Health Science Research Group for funding assistance.

BIBLIOGRAPHY

1 WHO, *WHO*, 2002.
2 L. Curtis, W. Rea, P. Smith-Willis, E. Fenyves and Y. Pan, *Environ. Int.*, 2006, 32, 815–830.
3 M. Kampa and E. Castanas, *Environ. Pollut.*, 2008, 151, 362–367.
4 Ł. Adamkiewicz, A. J. Badyda, A. Gayer and D. Mucha, *Adv. Exp. Med. Biol.*, 2015, 834, 15–20.
5 E. Liu, T. Yan, G. Birch and Y. Zhu, *Sci. Total Environ.*, 2014, 476–477, 522–531.
6 S. Martin, E. Fernandez-Alanis, V. Delfosse, P. Evelson, J. S. Yakisich, P. H. Saldiva and D. R. Tasat, *Inhal. Toxicol.*, 2010, 22, 1064–1071.
7 W. Yang and S. T. Omaye, *Mutat. Res. Toxicol. Environ. Mutagen.*, 2009, 674, 45–54.
8 Y. F. Zhu, T. Kuhn, P. Mayo and W. C. Hinds, *Environ. Sci. Technol.*, 2006, 40, 2531–2536.
9 V. Verma, T. Fang, H. Guo, L. King, J. T. Bates, R. E. Peltier, E. Edgerton, A. G. Russell and R. J. Weber, *Atmos Chem Phys*, 2014, 14, 12915–12930.
10 N. Daher, N. A. Saliba, A. L. Shihadeh, M. Jaafar, R. Baalbaki, M. M. Shafer, J. J. Schauer and C. Sioutas, *Sci. Total Environ.*, 2014, 470-471, 417–426.
11 F. M. Arantes-Costa, F. D. T. Q. S. Lopes, A. C. Toledo, P. A. Magliarelli-Filho, H. T. Moriya, R. Carvalho-Oliveira, T. Mauad, P. H. N. Saldiva and M. A. Martins, *Toxicol. Pathol.*, 2008, 36, 680–686.
12 J. J. Schauer, G. C. Lough, M. M. Shafer, W. F. Christensen, M. F. Arndt, J. T. DeMinter and J.-S. Park, *Res. Rep. Health Eff. Inst.*, 2006, 1–76; discussion 77–88.
13 M. R. Riley, D. E. Boesewetter, A. M. Kim and F. P. Sirvent, *Toxicology*, 2003, 190, 171–184.
14 J. Zhao, N. Lewinski and M. Riediker, *Aerosol Sci. Technol.*, 2015, 49, 65–74.
15 J. J. Schauer, B. J. Majestic, R. J. Sheesley, M. M. Shafer, J. T. Deminter, M. Mieritz and HEI Health Review Committee, *Res. Rep. Health Eff. Inst.*, 2010, 3–75; discussion 77–89.
16 F. J. Kelly, *Occup. Environ. Med.*, 2003, 60, 612–616.
17 S. K. Jalmi and A. K. Sinha, *Front. Plant Sci.*, 2015, 6, 769.
18 R. Foncea, C. Carvajal, C. Almarza and F. Leighton, *Biol. Res.*, 2000, 33, 89–96.
19 N. Li, J. Alam, M. I. Venkatesan, A. Eiguren-Fernandez, D. Schmitz, E. Di Stefano, N. Slaughter, E. Killeen, X. Wang, A. Huang, M. Wang, A. H. Miguel, A. Cho, C. Sioutas and A. E. Nel, *J. Immunol. Baltim. Md 1950*, 2004, 173, 3467–3481.
20 L. Fialkow, Y. Wang and G. P. Downey, *Free Radic. Biol. Med.*, 2007, 42, 153–164.
21 K. E. Iles and H. J. Forman, *Immunol. Res.*, 2002, 26, 95–105.
22 H. J. Forman and M. Torres, *Iubmb Life*, 2001, 51, 365–371.
23 A. P. Landreman, M. M. Shafer, J. C. Hemming, M. P. Hannigan and J. J. Schauer, *Aerosol Sci. Technol.*, 2008, 42, 946–957.
24 M. M. Shafer, D. A. Perkins, D. S. Antkiewicz, E. A. Stone, T. A. Quraishi and J. J. Schauer, *J. Environ. Monit.*, 2010, 12, 704–715.
25 M. S. Happo, R. O. Salonen, A. I. Hälinen, P. I. Jalava, A. S. Pennanen, J. a. M. A. Dormans, M. E. Gerlofs-Nijland, F. R. Cassee, V.-M. Kosma, M. Sillanpää, R. Hillamo and M.-R. Hirvonen, *Inhal. Toxicol.*, 2010, 22, 402–416.
26 S. J. Snow, A. De Vizcaya-Ruiz, A. Osornio-Vargas, R. F. Thomas, M. C. Schladweiler, J. McGee and U. P. Kodavanti, *J. Toxicol. Environ. Health A*, 2014, 77, 1164–1182.
27 T. Torvela, O. Uski, T. Karhunen, A. Lähde, P. Jalava, O. Sippula, J. Tissari, M.-R. Hirvonen and J. Jokiniemi, *Chem. Res. Toxicol.*, 2014, 27, 1516–1527.

28 J. Brocato, H. Sun, M. Shamy, T. Kluz, M. A. Alghamdi, M. I. Khoder, L.-C. Chen and M. Costa, *J. Toxicol. Environ. Health A*, 2014, 77, 751–766.
29 Z. Sijan, D. S. Antkiewicz, J. Heo, N. Y. Kado, J. J. Schauer, C. Sioutas and M. M. Shafer, *Environ. Toxicol.*, 2014, n/a–n/a.
30 A. Saffari, N. Daher, M. M. Shafer, J. J. Schauer and C. Sioutas, *Environ. Sci. Technol.*, 2014, 48, 7576–7583.
31 T. Okuda, J. J. Schauer and M. M. Shafer, *Atmos. Environ.*, 2014, 97, 552–555.
32 M. M. Shafer, B. M. Toner, J. T. Overdier, J. J. Schauer, S. C. Fakra, S. Hu, J. D. Herner and A. Ayala, *Environ. Sci. Technol.*, 2012, 46, 189–195.
33 S. Hu, J. D. Herner, M. Shafer, W. Robertson, J. J. Schauer, H. Dwyer, J. Collins, T. Huai and A. Ayala, *Atmos. Environ.*, 2009, 43, 2950–2959.
34 J. G. Charrier and C. Anastasio, *Atmos Chem Phys*, 2012, 12, 9321–9333.
35 A. K. Cho, C. Sioutas, A. H. Miguel, Y. Kumagai, D. A. Schmitz, M. Singh, A. Eiguren-Fernandez and J. R. Froines, *Environ. Res.*, 2005, 99, 40–47.
36 R. J. Delfino, N. Staimer, T. Tjoa, M. Arhami, A. Polidori, D. L. Gillen, S. C. George, M. M. Shafer, J. J. Schauer and C. Sioutas, *Epidemiology*, 2010, 21, 892–902.
37 S. Wittkopp, N. Staimer, T. Tjoa, T. Stinchcombe, N. Daher, J. J. Schauer, M. M. Shafer, C. Sioutas, D. L. Gillen and R. J. Delfino, *J. Expo. Sci. Environ. Epidemiol.*, 2015.
38 S. M. Platt, I. E. Haddad, S. M. Pieber, R.-J. Huang, A. A. Zardini, M. Clairotte, R. Suarez-Bertoa, P. Barmet, L. Pfaffenberger, R. Wolf, J. G. Slowik, S. J. Fuller, M. Kalberer, R. Chirico, J. Dommen, C. Astorga, R. Zimmermann, N. Marchand, S. Hellebust, B. Temime-Roussel, U. Baltensperger and A. S. H. Prévôt, *Nat. Commun.*, 2014, 5, 3749.
39 A. Saffari, S. Hasheminassab, D. Wang, M. M. Shafer, J. J. Schauer and C. Sioutas, *Atmos. Environ.*, 2015, 120, 286–296.
40 A. De Vizcaya-Ruiz, M. E. Gutiérrez-Castillo, M. Uribe-Ramirez, M. E. Cebrián, V. Mugica-Alvarez, J. Sepúlveda, I. Rosas, E. Salinas, C. Garcia-Cuéllar, F. Martínez, E. Alfaro-Moreno, V. Torres-Flores, A. Osornio-Vargas, C. Sioutas, P. M. Fine, M. Singh, M. D. Geller, T. Kuhn, A. H. Miguel, A. Eiguren-Fernandez, R. H. Schiestl, R. Reliene and J. Froines, *Atmos. Environ.*, 2006, 40, Supplement 2, 583–592.
41 M. Steenhof, I. Gosens, M. Strak, K. J. Godri, G. Hoek, F. R. Cassee, I. S. Mudway, F. J. Kelly, R. M. Harrison, E. Lebret, B. Brunekreef, N. A. Janssen and R. H. Pieters, *Part. Fibre Toxicol.*, 2011, 8, 26.
42 L. Ntziachristos, J. R. Froines, A. K. Cho and C. Sioutas, *Part. Fibre Toxicol.*, 2007, 4, 5.
43 T. Fang, V. Verma, H. Guo, L. E. King, E. S. Edgerton and R. J. Weber, *Atmos Meas Tech*, 2015, 8, 471–482.
44 C. Samara, A. Kouras, K. Kaidoglou, E.-N. Emmanouil-Nikoloussi, C. Simou, M. Bousnaki and A. Kelessis, *Sci. Total Environ.*, 2015, 532, 327–336.
45 N. A. H. Janssen, A. Yang, M. Strak, M. Steenhof, B. Hellack, M. E. Gerlofs-Nijland, T. Kuhlbusch, F. Kelly, R. Harrison, B. Brunekreef, G. Hoek and F. Cassee, *Sci. Total Environ.*, 2014, 472, 572–581.
46 R. J. Delfino, C. Sioutas and S. Malik, *Environ. Health Perspect.*, 2005, 113, 934–946.
47 R. J. Delfino, N. Staimer, T. Tjoa, D. L. Gillen, J. J. Schauer and M. M. Shafer, *J. Expo. Sci. Environ. Epidemiol.*, 2013, 23, 466–473.

48 J. G. Charrier, N. K. Richards-Henderson, K. J. Bein, A. S. McFall, A. S. Wexler and C. Anastasio, *Atmos Chem Phys*, 2015, 15, 2327–2340.
49 J. Mirowsky, C. Hickey, L. Horton, M. Blaustein, K. Galdanes, R. E. Peltier, S. Chillrud, L. C. Chen, J. Ross, A. Nadas, M. Lippmann and T. Gordon, *Inhal. Toxicol.*, 2013, 25, 747–757.
50 D. Wang, P. Pakbin, M. M. Shafer, D. Antkiewicz, J. J. Schauer and C. Sioutas, *Atmos. Environ.*, 2013, 77, 301–310.
51 A. Saffari, N. Daher, M. M. Shafer, J. J. Schauer and C. Sioutas, *J. Environ. Sci. Health Part - ToxicHazardous Subst. Environ. Eng.*, 2014, 49, 441–451.
52 S.-L. Huang, W.-L. Cheng, C.-T. Lee, H.-C. Huang and C.-C. Chan, *J. Toxicol. Environ. Health A*, 2002, 65, 1261–1272.
53 M. D. Ferguson, C. Migliaccio and T. Ward, *Inhal. Toxicol.*, 2013, 25, 766–773.
54 I. Boldogh, A. Bacsi, B. K. Choudhury, N. Dharajiya, R. Alam, T. K. Hazra, S. Mitra, R. M. Goldblum and S. Sur, *J. Clin. Invest.*, 2005, 115, 2169–2179.

Figure and Table Captions

Fig. 1. ROS Activity of Unfiltered & Filtered PM Extracts: Sum of Size Fractions (per m^3). ZYM = Zymosan (positive reference control)

Fig. 2. Size Resolved ROS Aerosol Concentrations: Categorized by Site Type (per m^3). Median values are indicated by the narrower line within the box; mean values by the thicker line with the box. The 5^{th} and 95^{th} percentiles are indicated by the whiskers and values outside the 5^{th} and 95^{th} percentiles are shown by dots.

Fig. 3. Size Resolved ROS Aerosol Concentrations: Categorized by Site Type (per mg). Median values are indicated by the narrower line within the box; mean values by the thicker line with the box. The 5^{th} and 95^{th} percentiles are indicated by the whiskers and values outside the 5^{th} and 95^{th} percentiles are shown by dots.

Fig. 4. DTT Activity of Unfiltered & Filtered PM Extracts: Sum of Size Fractions (per m^3)

Fig. 5. Size Resolved DTT Aerosol Concentrations: Categorized by Site Type (per m^3). Median values are indicated by the narrower line within the box; mean values by the thicker line with the box. The 5^{th} and 95^{th} percentiles are indicated by the whiskers and values outside the 5^{th} and 95^{th} percentiles are shown by dots.

Fig. 6. Size Resolved DTT Aerosol Concentrations: Categorized by Site Type (per mg). Median values are indicated by the narrower line within the box; mean values by the thicker line with the box. The 5^{th} and 95^{th} percentiles are indicated by the whiskers and values outside the 5^{th} and 95^{th} percentiles are shown by dots.

Fig. 7. Size Resolved ROS Activity: % of Total Activity. Sites Pooled. Median values are indicated by the narrower line within the box; mean values by the thicker line with the box. The 5^{th} and 95^{th} percentiles are indicated by the whiskers and values outside the 5^{th} and 95^{th} percentiles are shown by dots.

Fig. 8. Size Resolved DTT Activity: % of Total Activity. Sites Pooled. Median values are indicated by the narrower line within the box; mean values by the thicker line with the box. The 5^{th} and 95^{th} percentiles are indicated by the whiskers and values outside the 5^{th} and 95^{th} percentiles are shown by dots.Fig. 9. ROS Activity: µg ZYM/mg. Unfiltered Extracts. Sites Pooled. Median values are indicated by the narrower line within the box; mean values by the thicker line with the box. The 5^{th} and 95^{th} percentiles are indicated by the whiskers and values outside the 5^{th} and 95^{th} percentiles are shown by dots.

Fig. 10. DTT Activity: nmole/min/mg. Unfiltered Extracts. Sites Pooled. Median values are indicated by the narrower line within the box; mean values by the thicker line with the box. The 5^{th} and 95^{th} percentiles are indicated by the whiskers and values outside the 5^{th} and 95^{th} percentiles are shown by dots.

Fig. 11. ROS Activity: % in Filterable Fraction. Sites Pooled. Median values are indicated by the narrower line within the box; mean values by the thicker line with the box. The 5th and 95th percentiles are indicated by the whiskers and values outside the 5th and 95th percentiles are shown by dots.

Fig. 12. DTT Activity: % in Filterable Fraction. Sites Pooled. Median values are indicated by the narrower line within the box; mean values by the thicker line with the box. The 5th and 95th percentiles are indicated by the whiskers and values outside the 5th and 95th percentiles are shown by dots.

Table 1. PM-induced TNFα production in rat alveolar macrophages in six major cities and three rural locations in Europe.

Table 2. Spearman Correlation Coefficients between total element content of PM and ROS and DTT activity in unfiltered extracts of size-resolved PM.

Table 1

TNFα production in rat alveolar macrophages (AMs) exposed to PM from six major cities and three rural locations in Europe. Total and Filtered PM_3 and PM_{3-7} extracts were incubated with AMs for 6h. ELISA measurements of TNFα were normalized to PM mass and air volume (m^3). Data presented as mean ±standard deviation. "--" signifies missing data due to insufficient sample volumes.

Sampling Location	pg TNFα/mg PM				ng TNFα/m^3 air			
	PM_3 Total	PM_3 Filtered	PM_{3-7} Total	PM_{3-7} Filtered	PM_3 Total	PM_3 Filtered	PM_{3-7} Total	PM_{3-7} Filtered
AMSDM UB	3,973	303	--	--	50,610	3,863	--	--
± SD	74	92			944	1,176		
FRANK UB	8,671	447	--	--	73,127	3,771	--	--
± SD	82	8			695	64		
LONDN UB	--	--	4,542	425	--	--	11,605	1,086
± SD			41	5			105	12
LONDN UC	10,922	193	--	--	525,269	9,293	--	--
± SD	392	9			18,838	409		
MILAN UBI	2,144	217	6,058	440	68,937	6,980	15,745	1,142
± SD	133	7	328	15	4,263	210	853	39
STOCK UB	3,426	591	2,038	155	25,998	4,483	4,457	340
± SD	53	14	20	5	401	107	43	11
THESS UB	28,881	225	9,614	774	578,695	4,509	33,198	2,674
± SD	322	6	362	7	6,460	129	1,249	23
N-RURAL	754	100	--	--	7,444	989	--	--
± SD	21	2			203	18		
C-RURAL	1,405	153	198	155	11,701	1,278	513	401
± SD	91	20	3	2	757	167	7	6
S-RURAL	3,405	175	--	--	40,694	2,090	--	--
± SD	428	25			5,112	295		

Table 2

Spearman Correlation Coefficients between total element content of PM and ROS and DTT activity in unfiltered extracts of size-resolved PM. Twenty-eight most abundant elements ranked by median concentrations in bulk PM. Bolded (red) = r>0.70. Bolded italic (purple) = r>0.50.

Element	ROS			DTT		
	<3 µm	7-3 µm	>7 µm	<3 µm	7-3 µm	>7 µm
ROS	1.000	1.000	1.000	**0.929**	0.136	***0.691***
DTT	**.929**	0.136	***0.691***	1.000	1.000	1.000
Fe	-.221	-.082	.300	-.353	**.791**	***.545***
Ca	-.621	-.464	***.673***	-.535	.109	.391
Na	.400	.409	-.191	.338	.091	.064
S	***.571***	-.145	.091	***.585***	.036	.200
Al	-.118	***.564***	***.536***	-.256	.382	***.500***
K	.212	**.945**	.200	.050	.218	.309
Mg	-.015	***.609***	***.600***	-.044	.409	.491
P	.276	.445	.327	.259	-.018	.464
Ti	-.115	***.518***	***.545***	-.259	.427	***.627***
Zn	-.271	.264	.364	-.329	***.618***	***.564***
Cu	-.285	-.091	.173	-.391	**.764**	***.573***
Ba	-.188	-.064	.264	-.303	**.700**	***.536***
Mn	-.241	.055	**.727**	-.303	***.664***	***.618***
Cr	-.400	-.118	***.536***	-.474	***.545***	***.555***
Sn	-.156	.091	.255	-.268	**.791**	***.627***
Pb	-.056	-.264	***.636***	.135	***.536***	.464
Sr	-.088	.245	***.518***	-.129	***.573***	***.682***
Sb	-.244	-.127	.218	-.388	**.727**	***.555***
Ni	-.053	-.227	**.727**	-.062	.127	.291
B	-.350	-.082	.336	-.253	.182	.245
Mo	-.074	-.118	.136	-.279	***.682***	***.500***
V	.194	.164	***.655***	.103	.373	.427
Rb	.141	**.709**	.373	-.044	.382	.400
Ce	-.103	.336	.464	-.229	***.600***	***.564***
As	.388	-.009	**.709**	.382	***.591***	**.709**
La	.074	.218	.473	-.074	***.500***	***.609***
Li	-.015	***.609***	.373	-.124	.209	***.509***
Co	-.241	.173	***.636***	-.335	.491	***.564***

FIGURE 1

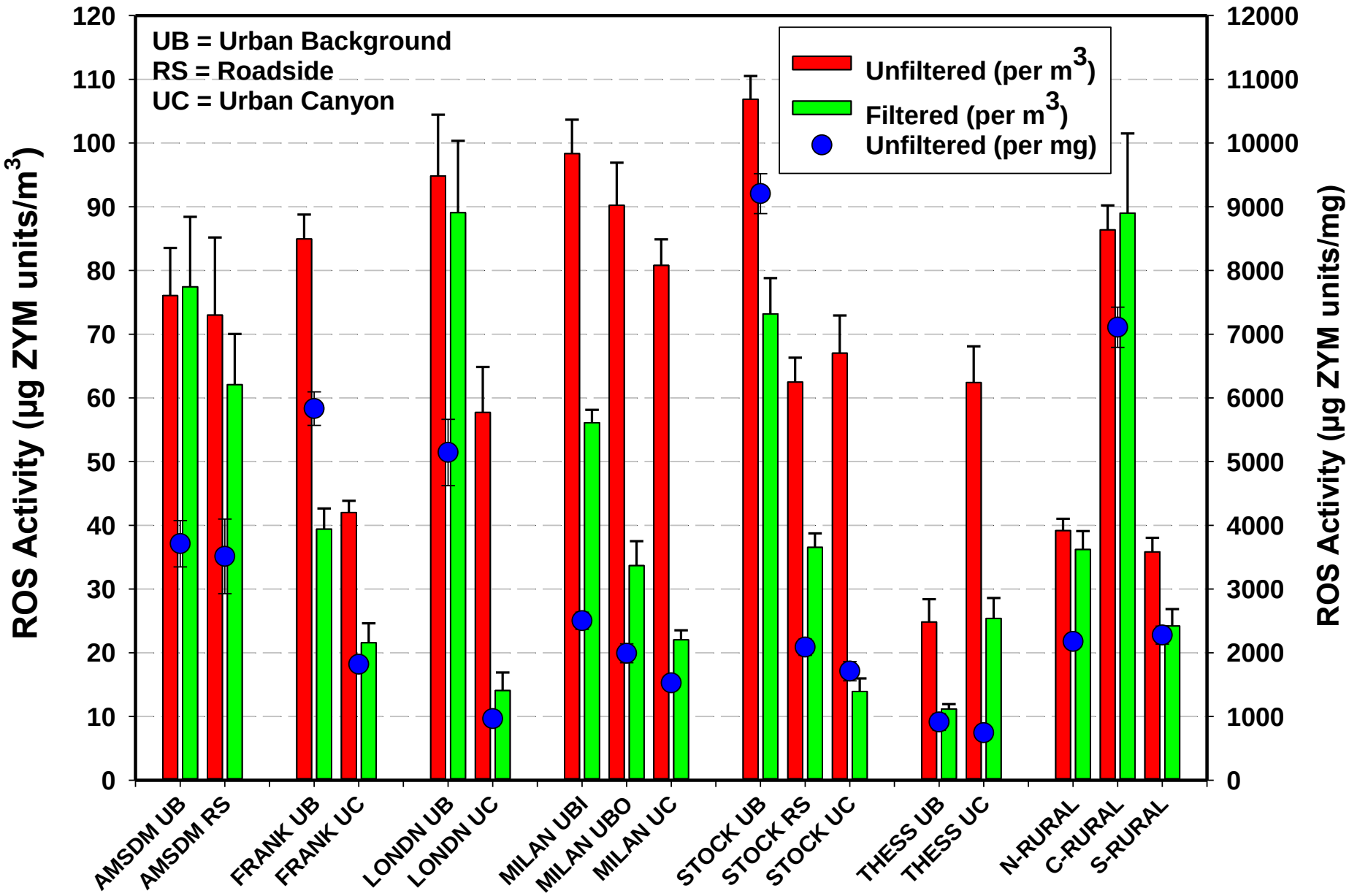
ROS Activity of Unfiltered & Filtered PM Extracts: Sum of Size Fractions
UB = Urban Background
RS = Roadside
UC = Urban Canyon
Unfiltered (per m3)
Filtered (per m3)
Unfiltered (per mg)
ROS Activity (µg ZYM units/m3)
ROS Activity (µg ZYM units/mg)
0
10
20
30
40
50
60
70
80
90
100
110
120
0
1000
2000
3000
4000
5000
6000
7000
8000
9000
10000
11000
12000
AMSDM UB
AMSDM RS
FRANK UB
FRANK UC
LONDN UB
LONDN UC
MILAN UBI
MILAN UBO
MILAN UC
STOCK UB
STOCK RS
STOCK UC
THESS UB
THESS UC
N-RURAL
C-RURAL
S-RURAL

FIGURE 2

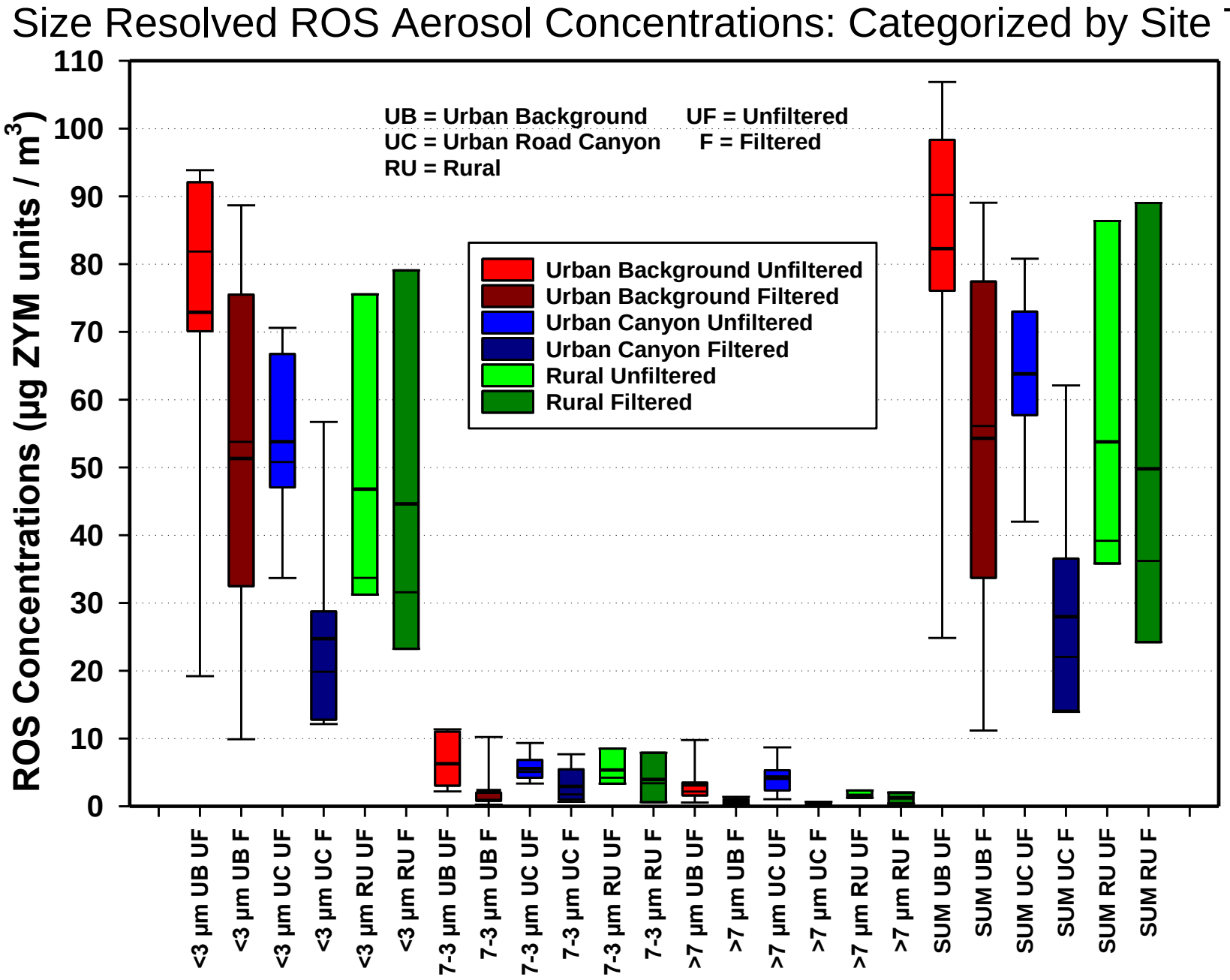
Size Resolved ROS Aerosol Concentrations: Categorized by Site Type
ROS Concentrations (µg ZYM units / m3)
UB = Urban Background
UC = Urban Road Canyon
RU = Rural
UF = Unfiltered
F = Filtered
Urban Background Unfiltered
Urban Background Filtered
Urban Canyon Unfiltered
Urban Canyon Filtered
Rural Unfiltered
Rural Filtered
0
10
20
30
40
50
60
70
80
90
100
110
<3 µm UB UF
<3 µm UB F
<3 µm UC UF
<3 µm UC F
<3 µm RU UF
<3 µm RU F
7-3 µm UB UF
7-3 µm UB F
7-3 µm UC UF
7-3 µm UC F
7-3 µm RU UF
7-3 µm RU F
>7 µm UB UF
>7 µm UB F
>7 µm UC UF
>7 µm UC F
>7 µm RU UF
>7 µm RU F
SUM UB UF
SUM UB F
SUM UC UF
SUM UC F
SUM RU UF
SUM RU F

FIGURE 3

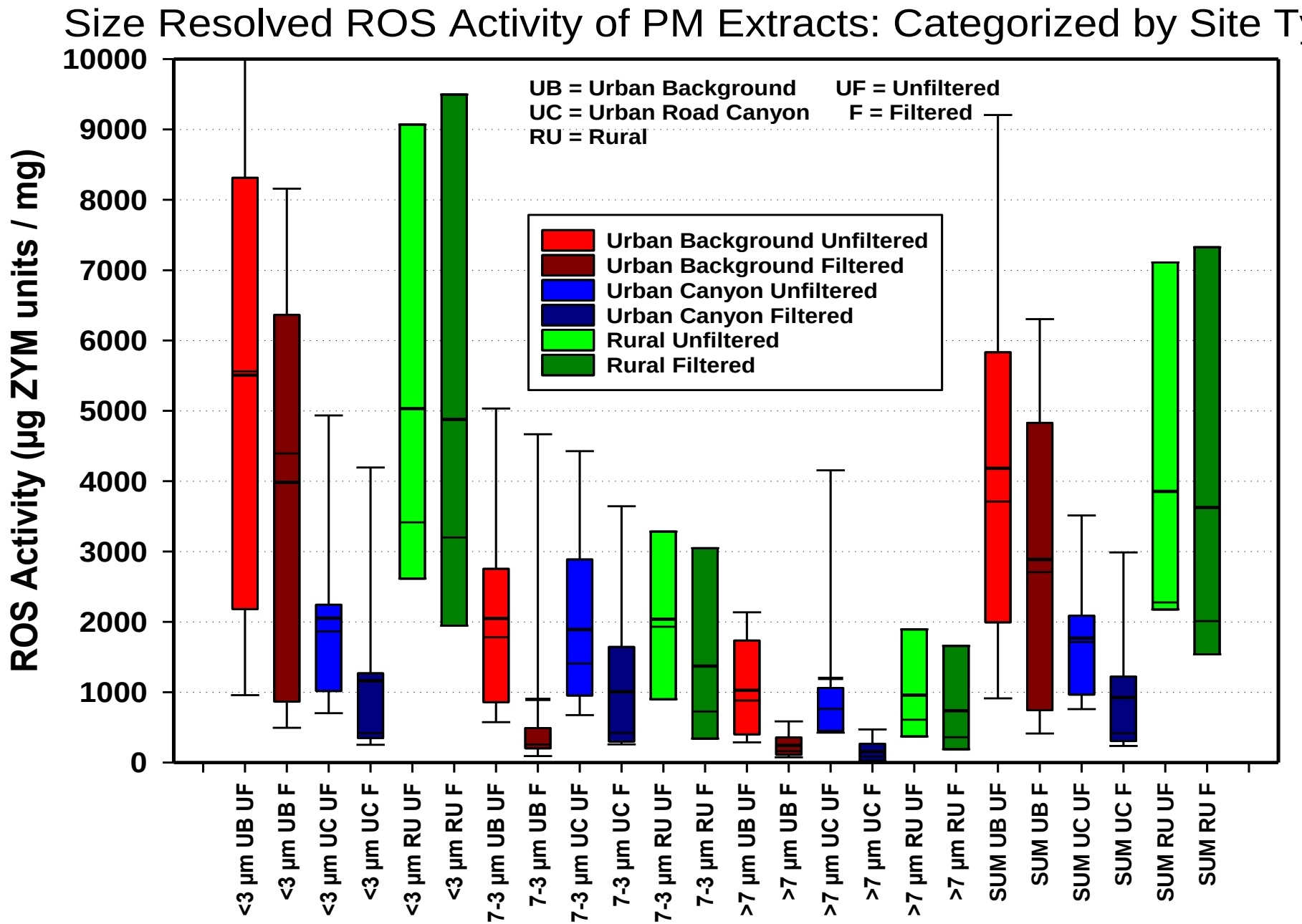
Size Resolved ROS Activity of PM Extracts: Categorized by Site Type
ROS Activity (µg ZYM units / mg)
10000
9000
8000
7000
6000
5000
4000
3000
2000
1000
0
UB = Urban Background
UC = Urban Road Canyon
RU = Rural
UF = Unfiltered
F = Filtered
Urban Background Unfiltered
Urban Background Filtered
Urban Canyon Unfiltered
Urban Canyon Filtered
Rural Unfiltered
Rural Filtered
<3 µm UB UF
<3 µm UB F
<3 µm UC UF
<3 µm UC F
<3 µm RU UF
<3 µm RU F
7-3 µm UB UF
7-3 µm UB F
7-3 µm UC UF
7-3 µm UC F
7-3 µm RU UF
7-3 µm RU F
>7 µm UB UF
>7 µm UB F
>7 µm UC UF
>7 µm UC F
>7 µm RU UF
>7 µm RU F
SUM UB UF
SUM UB F
SUM UC UF
SUM UC F
SUM RU UF
SUM RU F

FIGURE 4

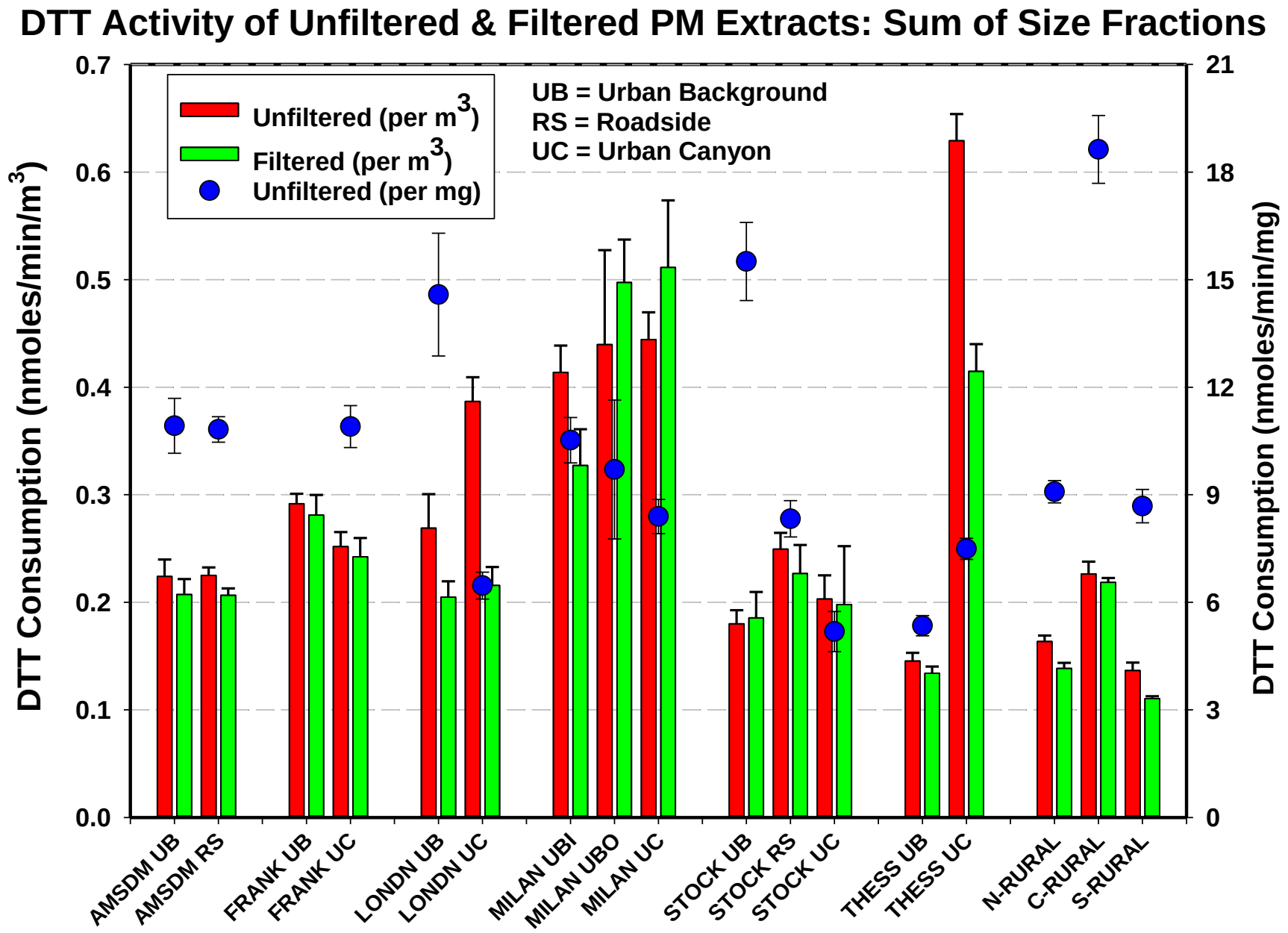
DTT Activity of Unfiltered & Filtered PM Extracts: Sum of Size Fractions
Unfiltered (per m3)
Filtered (per m3)
Unfiltered (per mg)
UB = Urban Background
RS = Roadside
UC = Urban Canyon
DTT Consumption (nmoles/min/m3)
DTT Consumption (nmoles/min/mg)
0.0
0.1
0.2
0.3
0.4
0.5
0.6
0.7
0
3
6
9
12
15
18
21
AMSDM UB
AMSDM RS
FRANK UB
FRANK UC
LONDN UB
LONDN UC
MILAN UBI
MILAN UBO
MILAN UC
STOCK UB
STOCK RS
STOCK UC
THESS UB
THESS UC
N-RURAL
C-RURAL
S-RURAL

FIGURE 5

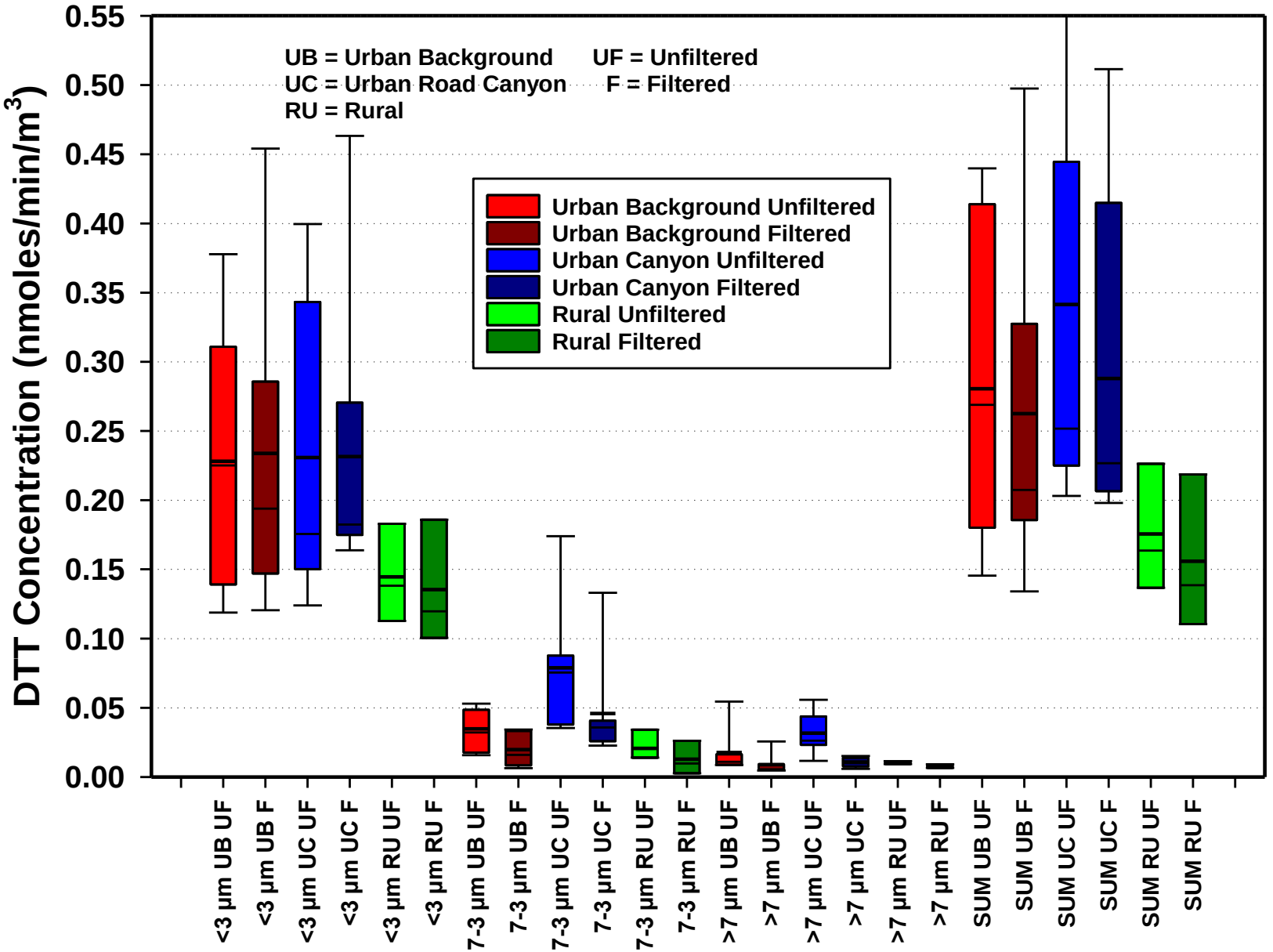
Size Resolved DTT Aerosol Concentrations: Categorized by Site Type
UB = Urban Background
UC = Urban Road Canyon
RU = Rural
UF = Unfiltered
F = Filtered
Urban Background Unfiltered
Urban Background Filtered
Urban Canyon Unfiltered
Urban Canyon Filtered
Rural Unfiltered
Rural Filtered
DTT Concentration (nmoles/min/m3)
0.55
0.50
0.45
0.40
0.35
0.30
0.25
0.20
0.15
0.10
0.05
0.00
<3 µm UB UF
<3 µm UB F
<3 µm UC UF
<3 µm UC F
<3 µm RU UF
<3 µm RU F
7-3 µm UB UF
7-3 µm UB F
7-3 µm UC UF
7-3 µm UC F
7-3 µm RU UF
7-3 µm RU F
>7 µm UB UF
>7 µm UB F
>7 µm UC UF
>7 µm UC F
>7 µm RU UF
>7 µm RU F
SUM UB UF
SUM UB F
SUM UC UF
SUM UC F
SUM RU UF
SUM RU F

FIGURE 6

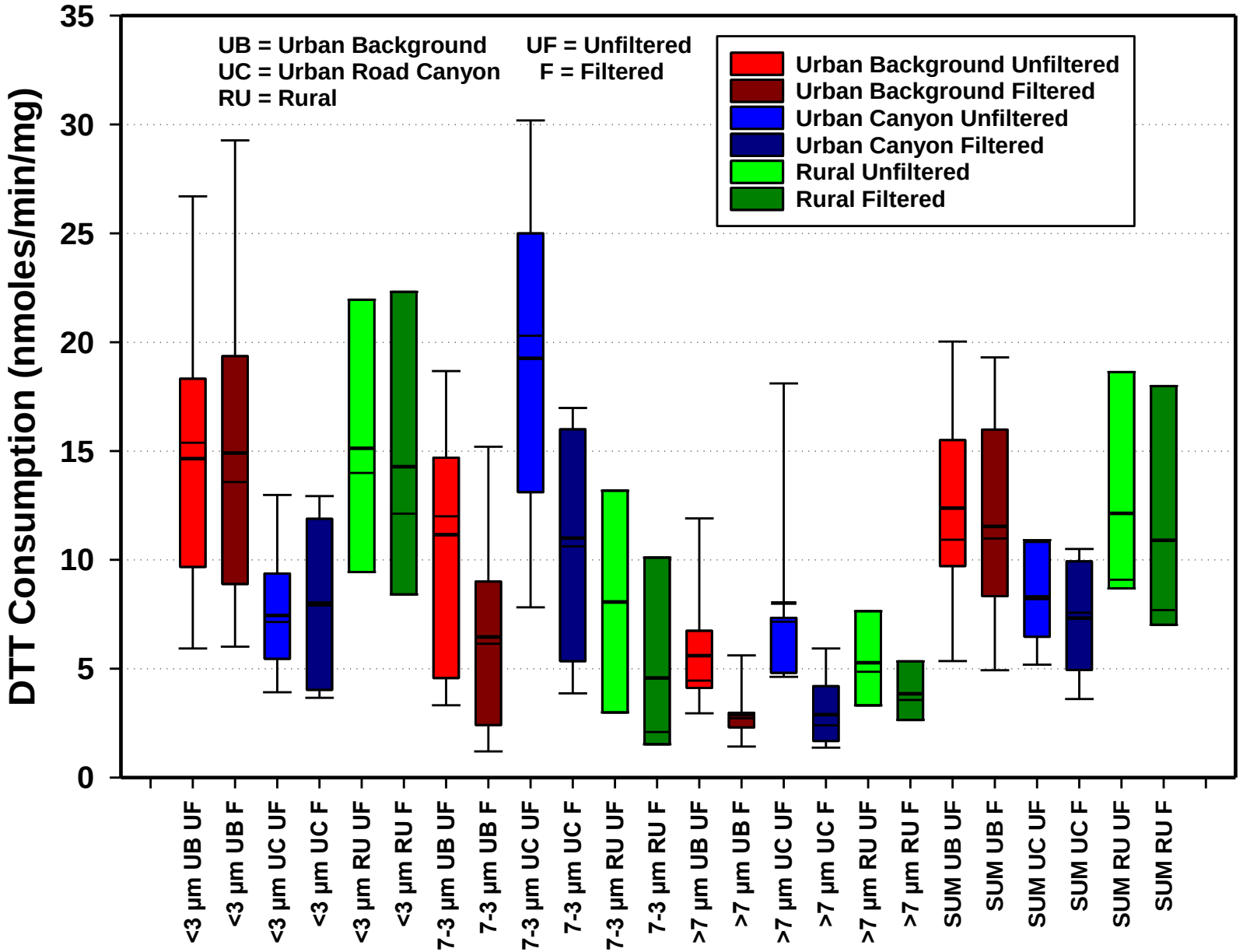
Size Resolved DTT Activity of PM Extracts: Categorized by Site Type
UB = Urban Background
UC = Urban Road Canyon
RU = Rural
UF = Unfiltered
F = Filtered
Urban Background Unfiltered
Urban Background Filtered
Urban Canyon Unfiltered
Urban Canyon Filtered
Rural Unfiltered
Rural Filtered
DTT Consumption (nmoles/min/mg)
0
5
10
15
20
25
30
35
<3 µm UB UF
<3 µm UB F
<3 µm UC UF
<3 µm UC F
<3 µm RU UF
<3 µm RU F
7-3 µm UB UF
7-3 µm UB F
7-3 µm UC UF
7-3 µm UC F
7-3 µm RU UF
7-3 µm RU F
>7 µm UB UF
>7 µm UB F
>7 µm UC UF
>7 µm UC F
>7 µm RU UF
>7 µm RU F
SUM UB UF
SUM UB F
SUM UC UF
SUM UC F
SUM RU UF
SUM RU F

FIGURE 7

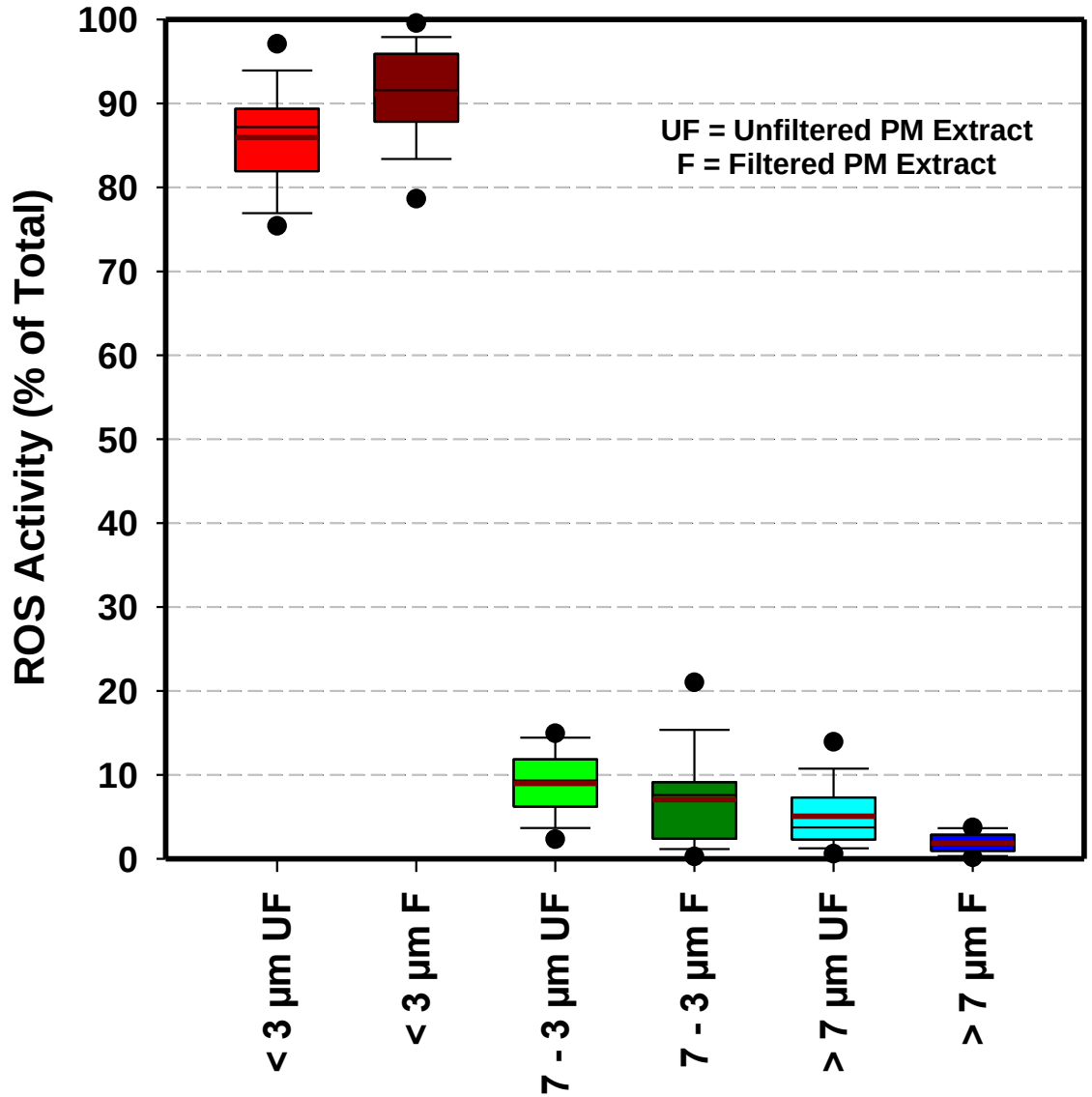
Size Resolved ROS Activity: % of Total. Sites Pooled
ROS Activity (% of Total)
100
90
80
70
60
50
40
30
20
10
0
UF = Unfiltered PM Extract
F = Filtered PM Extract
< 3 µm UF
< 3 µm F
7 - 3 µm UF
7 - 3 µm F
> 7 µm UF
> 7 µm F

FIGURE 8

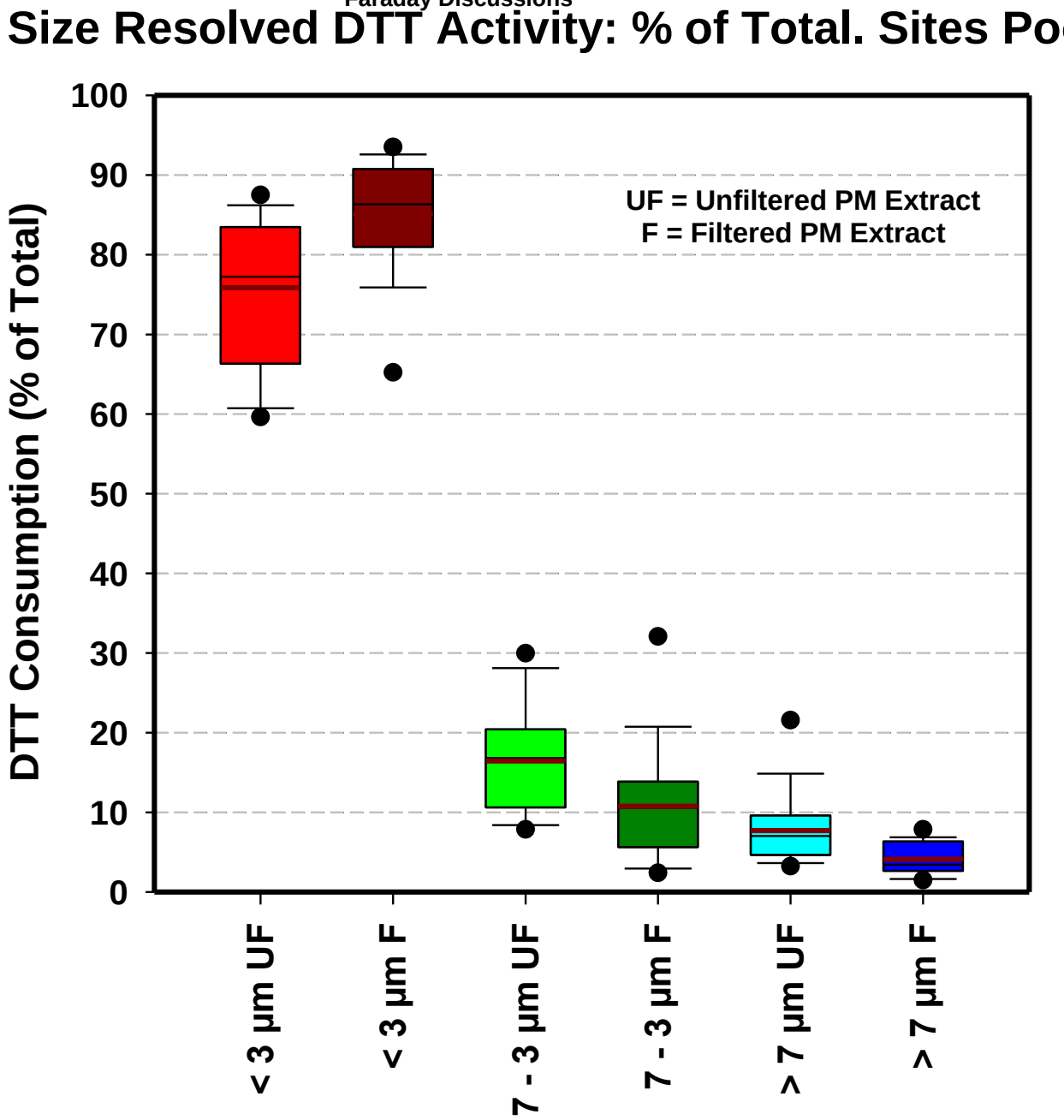
Size Resolved DTT Activity: % of Total. Sites Pooled
DTT Consumption (% of Total)
100
90
80
70
60
50
40
30
20
10
0
UF = Unfiltered PM Extract
F = Filtered PM Extract
< 3 µm UF
< 3 µm F
7 - 3 µm UF
7 - 3 µm F
> 7 µm UF
> 7 µm F

FIGURE 9

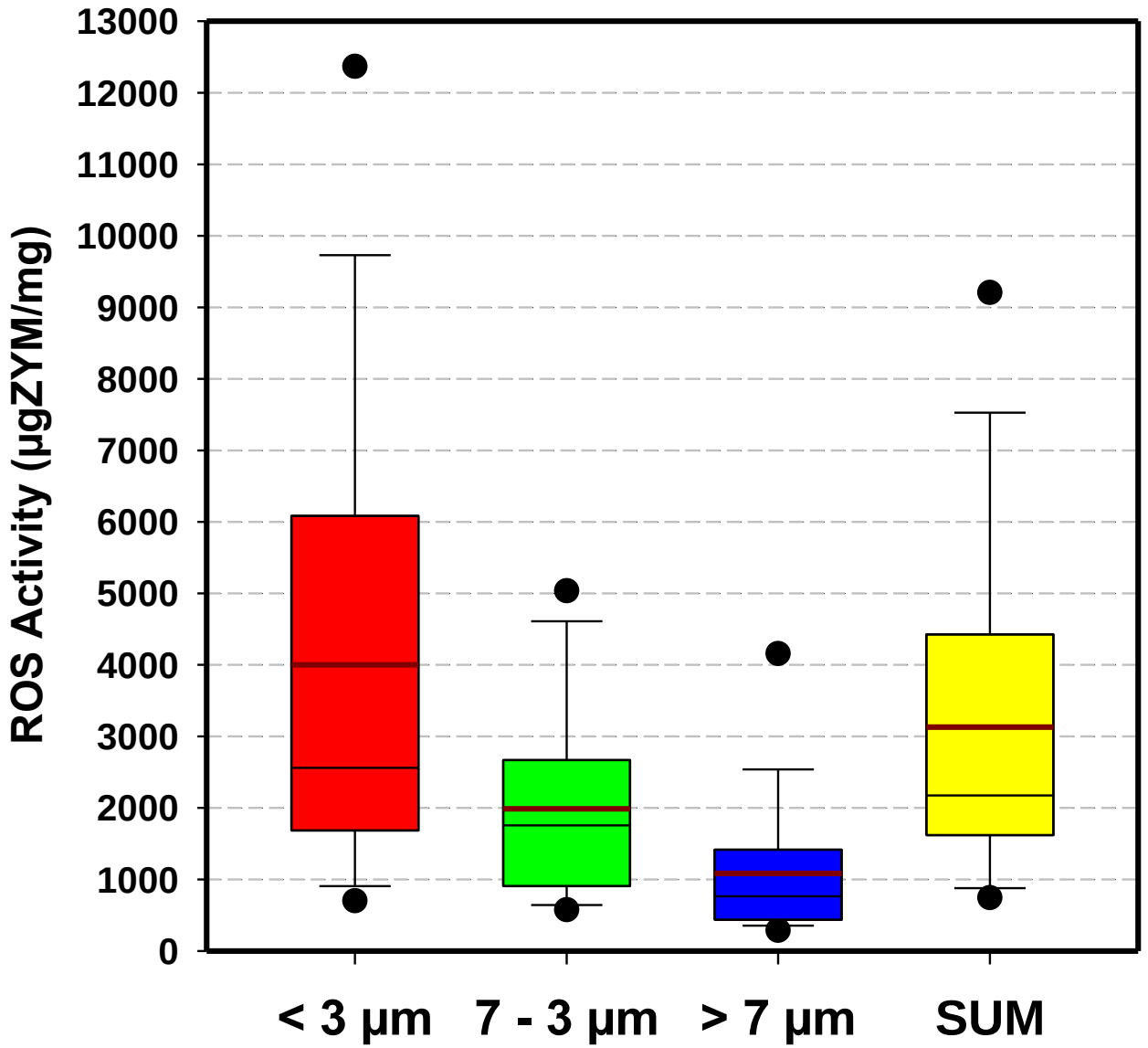
ROS Activity: µg ZYM/mg. Unfiltered Extract. Sites Pooled
ROS Activity (µgZYM/mg)
13000
12000
11000
10000
9000
8000
7000
6000
5000
4000
3000
2000
1000
0
< 3 µm
7 - 3 µm
> 7 µm
SUM

FIGURE 10

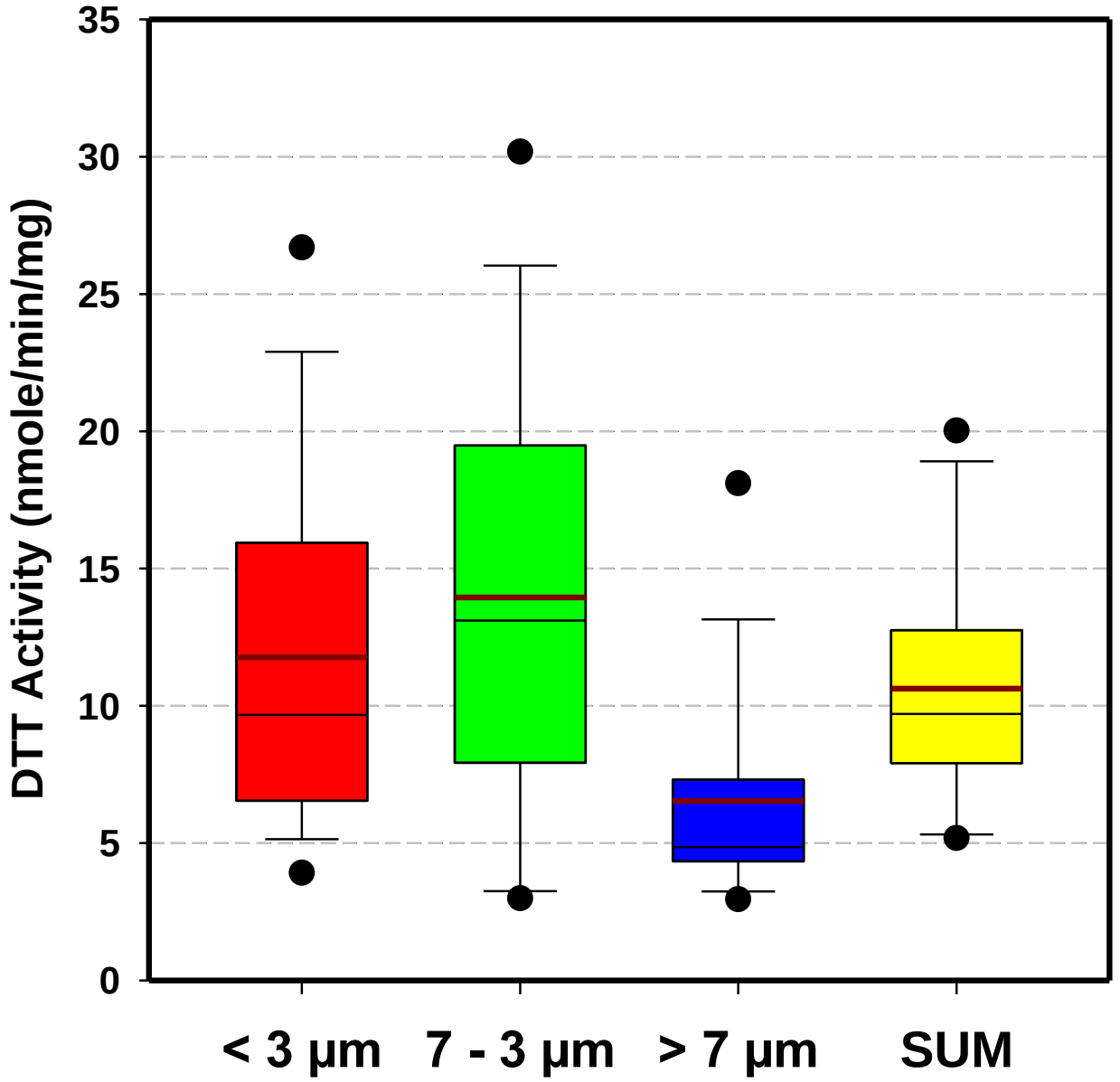
DTT Activity: nmole/min/mg. Unfiltered Extract. Sites Pooled
DTT Activity (nmole/min/mg)
35
30
25
20
15
10
5
0
< 3 µm
7 - 3 µm
> 7 µm
SUM

FIGURE 11

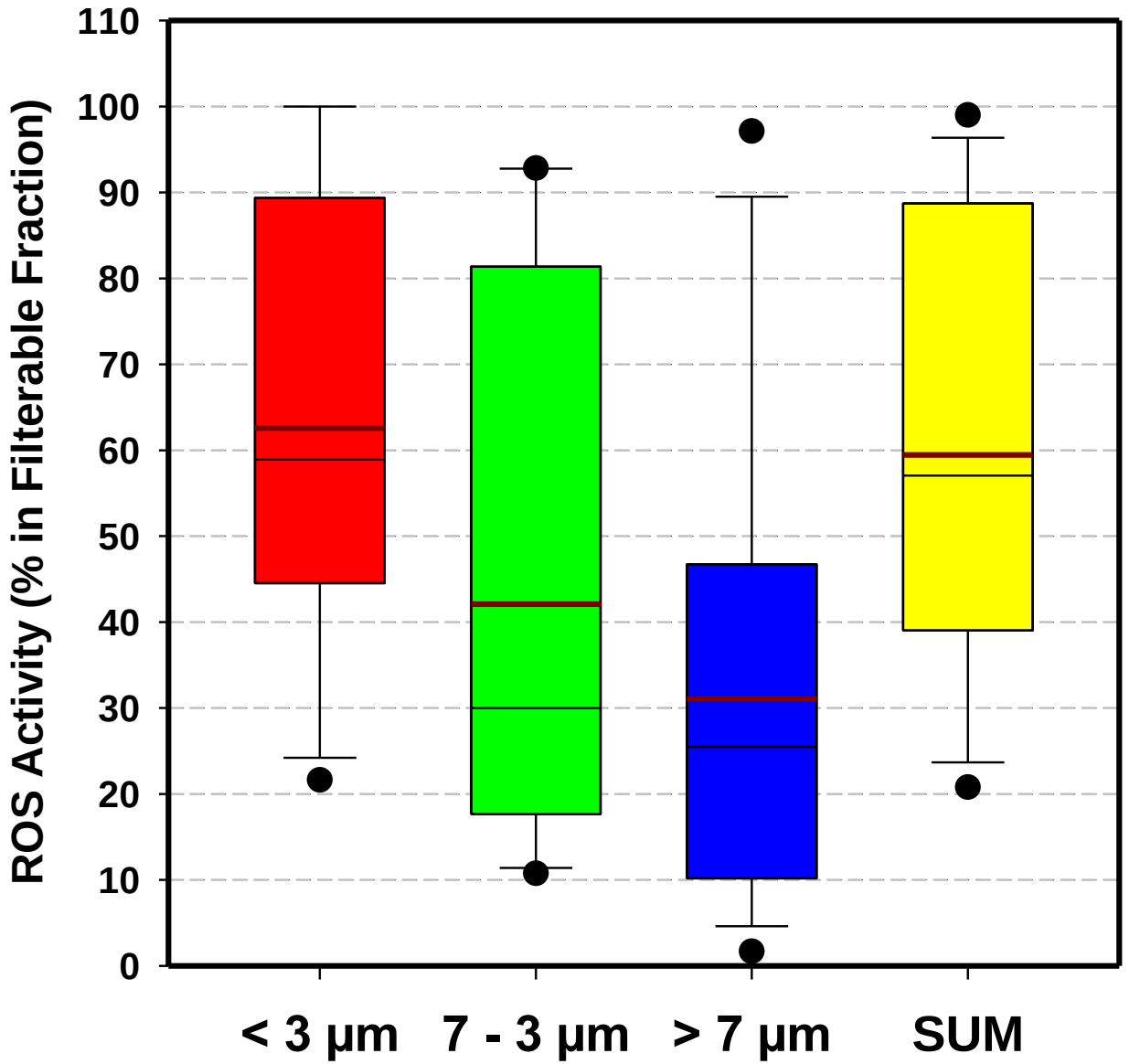
ROS Activity: % in Filterable Fraction. Sites Pooled
ROS Activity (% in Filterable Fraction)
110
100
90
80
70
60
50
40
30
20
10
0
< 3 µm
7 - 3 µm
> 7 µm
SUM

FIGURE 12

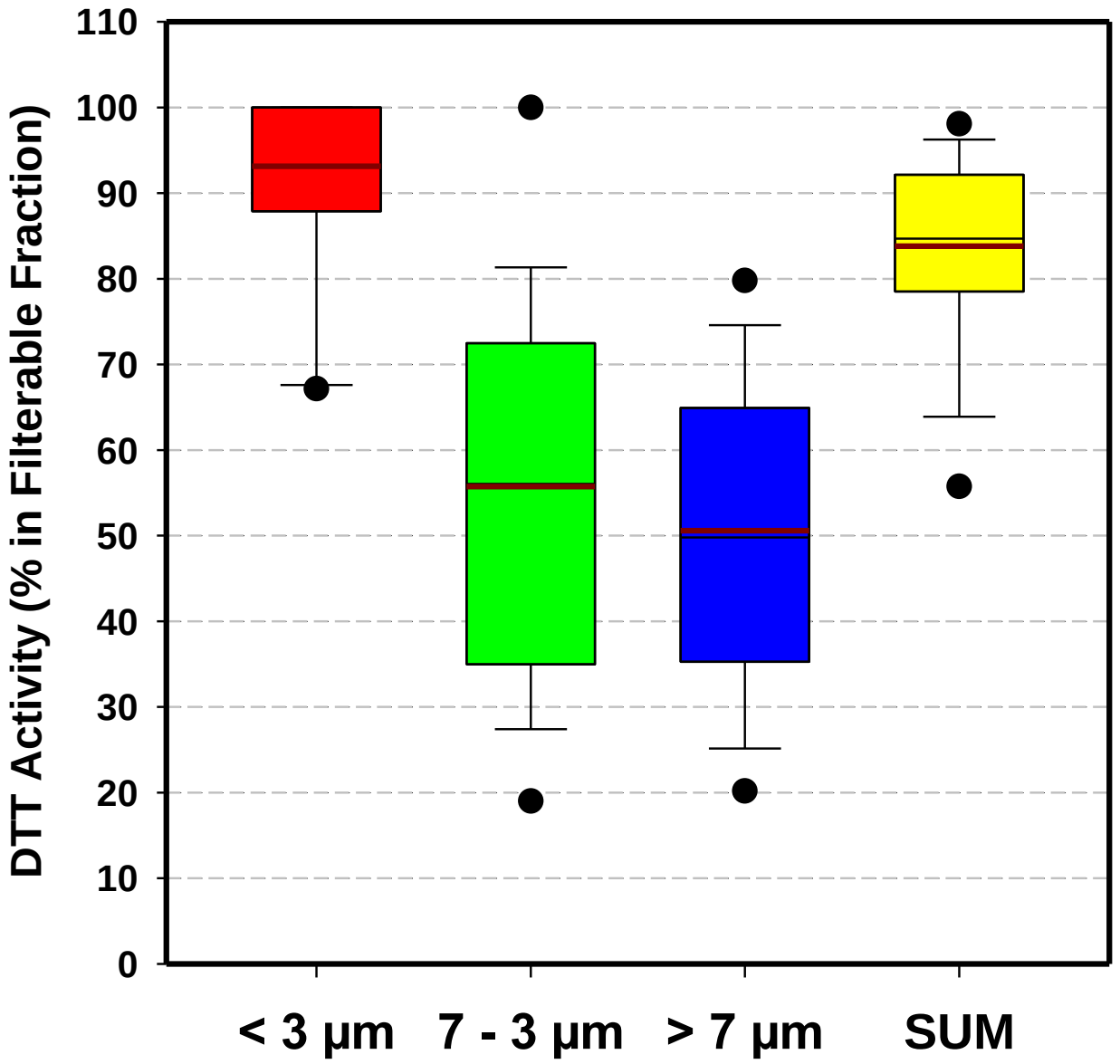
DTT Activity: % in Filterable Fraction. Sites Pooled
DTT Activity (% in Filterable Fraction)
110
100
90
80
70
60
50
40
30
20
10
0
< 3 µm
7 - 3 µm
> 7 µm
SUM